Treball de Fi de Màster

Màster Universitari en Enginyeria Industrial

Modelling, control and simulation of LCC-HVDC systems for stability studies

Autor: Joaquín Rebled Lluch
Co-Director: Eduardo Prieto Araujo
Director: Oriol Gomis Bellmunt

Convocatòria: Juny 2017

Escola Tècnica Superior
d'Enginyeria Industrial de Barcelona

Abstract

El present treball de final de màster presenta la modelització, control i simulació d'un sistema LCC-HVDC, corresponent a la tecnologia HVDC més prevalent en xarxes de transport d'alta tensió.

Es realitza una anàlisi teòrica del funcionament del procés de commutació, per aclarir els fonaments sobre les quals es basa el LCC. Aquesta anàlisi es completa mitjançant un estudi de les corbes estàtiques del sistema, per comprendre la resposta del LCC-HVDC en estat estacionari. Aleshores, es desenvolupa un model de petit senyal del sistema de tranmissió, que inclou el LCC-HVDC i les xarxes AC pròximes a cadascun dels terminals del sistema.

Finalment, es valida el model de petit senyal mitjançant una comparativa amb la resposta del model no-lineal del sistema. S'estudia l'effecta del rati de curtcircuit on les dinàmiques del sistema, així com la resposta en front a canvis de referència. Totes les simulacions es realitzant en el entorn MATLAB®-Simulink.

This Master Thesis present the modelling, control and simulation of a LCC-HVDC (Line-Commutated Converter, High Voltage Direct Current), which is the most prevalent type of HVDC technology in current transmission grids.

An analysis of the commutation process is performed, illustrating the base theory behind an LCC. The analysis follows with the static characteristic curves of the LCC-HVDC transmission system, to understand the system operation in steady-state. Furthermore, a small-signal model of the transmission system is developed, including the AC system at the rectifier and inverter terminals.

The small-signal model is validated by comparison with the non-linear model of the system. The effect of the short-circuit ratio (SCR) on the system performance is also studied, as well as the system response to reference changes. All simulations are performed within MATLAB®-Simulink environment.

Contents

List of Figures

List of Tables

Preface

Due to the penetration of renewable energy systems and power electronics in High Voltage (HV) grids, particularly High Voltage Direc Current (HVDC)-focused power electronics, TSOs are increasingly worried about stability issues. Additionally, traditional stability theory may not be accurate nor appropriate in grids with a high penetration of power electronics.
Line-Commutated Converters (LCC) are one of the basic types of converters that have a strong presence in modern grids. For this reason, having an accurate small-signal model of an LCC converter is a necessary step before performing stability studies implicating multiple power electronic systems. In fact, the model constructed in this project will be one of the basic blocks employed in an ongoing project, sponsored by the spanish Transmission System Operator (TSO). At the end of this project, this model will be employed along with other models in small-signal stability studies, in order to anticipate potentially harmful situation that could compromise the Spanish grid stability. Additionally, the control interactions between different power electronic systems will be studied thanks to this model, along with other tools. Therefore, this Master's Thesis is considered a first step towards a future PhD focused around interactions between power electronics in high-voltage AC/DC systems.

Chapter 1

Introduction

1.1 Introduction

Although that during twentieth century alternating current was the main method of power transmission, HVDC technology has proven to be the best solution for some specific applications. From 1970 onwards, the number of installations with this technology has been growing steadily. According to [1], the worldwide number of HVDC connections was 170 in 2015, and the largest can operate at a voltage of ±800 kV and a maximum current of 4500 A. HVDC technology is preferred in general for the following applications:

- Long distance bulk power transmission with overhead lines;
- Submarine or underground power transmission;
- Link between AC systems at different frequencies or phase;
- Power transmission for isolated generation units such as offshore wind farms or oil rigs.

Among HVDC application, two technologies arise at different times. In 1954 [2], the first HVDC point-to-point was made available by the use of mercury-arc valves. This technology was used during this first years of HVDC, but was subsequently displaced by the use of power transistors, such as thyristors from the 1970s or insulated-gate bipolar transistors (IGBT) from the 1990s.

1.1.1 HVDC systems advantages over HVAC

Since transformers made AC systems won the war of currents in early 20th century, AC has been the preferred method for power transmission. Direct current has been mostly relegated for years to other fields, such as electronics and some chemical industrial processes. However, starting from the 1970s [2], DC started to be considered an interested method for bulk power transmission. AC systems present some disadvantages, related to reactive capacitive power and its consequences on power transmission capability, particularly when transmitting larges amount of power through subsea cables.
DC systems, on the other hand, do not present any sort of reactive power. In fact, capacitive and

inductive effects are a consequence of the sinusoidal variations of voltage and current, as reactive power depends on the frequency. If voltage and current do not oscillate (i.e. the frequency is null), line inductance and line capacitance effects are null in steady state. Therefore, DC systems are only limited by ohmic losses, as inductive and capacitive effects are not present in steady-state. Consequently, there is no need to compensate the reactive power produced by the cables, lowering the transmission system cost. On the other hand, the absence of reactive power increases system stability, permitting power to be transmitted with a DC connection for very long distances [3].
Moreover, as skin and proximity effect are inherent to AC systems, they do not affect DC systems. Therefore, for two equivalent systems, the AC line resistance is higher than the DC one; hence, active (ohmic) losses in DC lines are lower. In fact, it is equivalent to say that the equivalent cross section between AC and DC is lower in the latter, which decreases cable costs. Besides that, direct current allows for different AC grids to be linked asynchronously. Therefore, it can help system stability and also prevent cascading failures, by stopping faults or overloads from propagating. Changes in load that would cause portions of an AC network to become unsynchronized and to separate, would not similarly affect a DC link, and the power flow through the DC link can be used to stabilize the AC network [4].

1.1.2 LCC-HVDC

Most of HVDC converters in operation are LCC [2]. Modern LCC are based on controllable switching devices, employing thyristor valves to perform the commutation. In a LCC, the DC current does not change its direction; it flows through a large inductance and can be considered almost constant. On the AC side, the converter behaves approximately as a current source, injecting both grid-frequency and harmonic currents into the AC network. For this reason, LCC for HVDC is also known as a current-source converter. Because the direction of current cannot be varied, reversal of the direction of power flow (when required) is achieved by reversing the polarity of DC voltage at both stations [5].
LCCs rely on a strong AC system to operate. In fact, an AC voltage is necessary to allow the commutation from one switching device to another. Consequently, LCCs depend upon a synchronous AC grid to ensure power conversion. Moreover, a line-commutated converter in steady-state operation at 1 p.u. (rated) active power will consume approximatively 0.5 p.u. of reactive power [6], which has to be compensated with capacitor banks, thus implying a larger substation size. Nevertheless, LCCs have lower losses than their counterpart - VSC converters - does; LCC losses are indeed reported as 0.7 % of the converted power [6].
Despite the lower losses, an LCC-HVDC substation needs much more space. Compared to a VSC-HVDC station, a complete LCC ones needs double the space [7]. This is mainly due to the need of capacitor banks as mentioned, and filter banks to cope with the harmonics. LCC converters generate harmonics, which are to be filtered; hence implying that there is need to accommodate filters in the substations. According to [7], an LCC substation in the hundred-MW range would need between 1600 and 5000 m^2 only for the filter banks. Additionally, LCC need a strong AC grid to properly commutate the current between the thyristor valves and it is not capable to provide black start capability.

1.1.3 VSC-HVDC

Alternatively, VSCs overcome most of the LCC challenges, and offer other significant advantages. It is an incipient technology; the first VSC converted being installed onshore in 1997. The use of those converters in offshore transmission is relatively new, as the first VSC converter was installed offshore in 2005. Back then they used two-level topologies, whereas nowadays, VSC employ modular multi-level converter (MMC) concepts. VSC are based on IGBT transistors, which are fully controllable - they can be turned both on and off - on contrary to the thyristors used in LCC converters. Furthermore, in VSCs the active and the reactive power can be controlled independently, so there is no need for reactive power compensation [8]. Additionally, in VSC converters reversal of the power flow is done by reversal of the current - again on the contrary to LCC converters, where the voltage polarity is inverted - thus making them more suitable for DC grid applications [9]. Moreover, as their AC voltage has a low harmonic content, the need for filters is greatly reduced or even eliminated.
Another factor which makes VSC converters more interesting is their black start capability. In case of a blackout, VSC converters can lead the grid restoration (provided its capacitors are charged and can function as a voltage source) as they are not dependent on an AC grid to function, nor require an external power supply. According to [4], VSC converters make restoration of the system more reliable and less complicated, by providing a stable frequency and voltage during the recovery process.
On the other hand, one of the main drawback of VSC converters is their losses. Initially, losses on the first VSC converter were reported as 3% of the converted power for the first designs. Nowadays, modern modular multi-level converters achieve less than 1% losses per converter [10].

1.2 Research question

There are available detailed models of VSC and VSC-MMC systems available on the literature. To the best of the author's knowledge, it is difficult to find disclosed small-signal models available for LCC-HVDC systems, despite being much more prevalent in nowadays grids. Moreover, from a stability point of view, LCC-HVDC systems are more complex to study as well as more prevalent in HV grids. Therefore, this thesis aims to respond to the need of providing with a disclosed and detailed small-signal LCC-HVDC system model, which could be the backbone of a future stability study on a larger scale.

1.3 Thesis goals

Relating to the problematic of this thesis, the goals are set as follows:

- To understand theoretical background of the LCC converter;
- To assimilate steady-state behaviour of the LCC-HVDC transmission system, related to operational static curves;
- To comprehend the dynamic response of the LCC-HVDC transmission system based on theoretical equations and a non-linear model, in order to build a small-signal model in a state-space representation;

- To verify the accuracy and adequacy of the small-signal model with a comparative case study;
- To identify issues related to hazardous dynamics, by analysing the results of the small-signal model, thus opening the way for future studies.

Moreover, it is necessary to test the small-signal model against similar models to ensure proper accuracy of the results.

1.4 Thesis scope

This thesis includes the analysis, modelling, control, and simulation of a monopolar LCC-HVDC transmission system. The construction of the model is the main contribution.

All simulations are performed using the 2015b version of MATLAB®-Simulink.

1.5 Thesis outline

This thesis is organized as follows:

- Chapter 2 shows the principal elements of an LCC-HVDC link and explains its main role as well as gives the theoretical background of the LCC converter, detailing the commutation process;
- Chapter 3 explores the static behaviour of a typical LCC-HVDC transmission system, which allows to understand the operational principles behind it;
- Chapter 4 studies the interactions between the AC and DC side of the LCC-HVDC transmission system, by means of the characteristic static curves;
- Chapter 5 explains the development of a small-signal model of an LCC-HVDC link, based in space state representation;
- Chapter 6 covers the testing of the small-signal model by comparing its outputs with a non-linear model, as well as performs a mathematical analysis of the linear model.

Chapter 2

LCC basic principles

2.1 Introduction

This sections aims to explain the theory behind an LCC converter, which will be used in the following chapters to study steady-state behaviour and to build the small-signal model.

2.2 Main elements of an LCC-HVDC transmision system

This sections aims to highlight the main elements of a 12-pulse monopole LCC-HVDC transmission system. Those elements will be modeled and accounted for in the small-signal analysis.

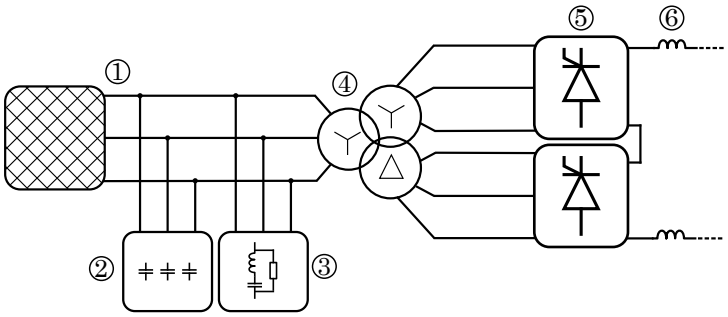

Figure 2.1: Schematic displaying the main elements of an LCC-HVDC transmission system

Previous figure displays a scheme of the basic elements forming a 12-pulse LCC HVDC transmission system. Only the rectifier pole is shown, but the inverter has the same arrangement and elements:

1. AC grid
   Although formed by an aggregation of generators, transformers and lines among other elements, the AC grid can be modelled by an ideal voltage source with a series impedance. The grid impedance represents the Thevenin equivalent circuit seen from the LCC rectifier. It is inversely proportional to the strength of the AC grid, i.e. a weak AC grid will

translate in a high equivalent grid impedance, therefore any change in current will imply strong voltage fluctuations. Another concept related with the strength of the AC grid is the short-circuit ratio (SCR) [5], which evaluates the strength of the AC grid relative to the power of the HVDC link. A SCR of 3.0 is generally defined as the bottom threshold of strong ac-grid operation, while SCR between 2.0 and 3.0 fall in the range of weak AC grid operation, in which case the HVDC system must undergo specific modifications (particularly regarding the control system) in order to avoid instabilities. For more details on the SCR, see section 4.4.1.

2. AC filters
   Converter operation results in both generation of AC current harmonics and absorption of reactive power. Switchable filters are responsible for mitigating current harmonics, as well as providing reactive power in conjunction with the capacitor banks.

   Tuned filters are generally employed to mitigate the stronger harmonics (corresponding to 11th and 13th in a 12-pulse bridge). Both single-tuned, double-tuned or triple-tuned filters can be employed. For higher-order harmonics damped high-pass filters are preferred.

3. Capacitor banks
   Capacitor banks are arranged such as to be able to generate the reactive power demanded by the converters. There are multiple switchable capacitor banks in order to adapt to the reactive demands of the converters. Their dynamics during AC voltage fluctuations are to be considered in order to prevent AC voltage instabilities.

4. Power Transformers
   Tap-changing power transformers used to control the voltage level of the AC-side of the converter. The regulation of the tap-changer is determined by the control mode.

   On the other hand, the use of a star-star-delta transformer allows for a phase shift of 30° (either 30°, -30°, 150°,...), which allows lower ripple and harmonic content.

   Sets of single-phase double-winding transformers are preferred, that is the configuration seen in the figure would require three single-phase star-star transformers and three single-phase star-delta transformers. The on-load tap changer would be allocated on the primary of each of the transformers.

5. HVDC converter
   The converters are the interface between the AC-side and DC-side of the system. Their operation is driven by gate pulses determined by the control system. More detail on the principle of LCC can be found in following sections.

6. DC reactor
   The DC reactor is normally required for power transmission schemes, and generally not for back-to-back schemes [1]. They provide a number of principal functions:

   - Reduce DC current ripple;
   - Reduce fault current;

- Ensure that the DC-side resonance frequencies are not multiples of the AC frequency;
- Protect the thyristor valves from fast transients originating on the DC transmission (e.g. a lighting strike).

2.3 Ideal diode bridge

A basic 6-pulse diode bridge is the first step to understand the working principle of the LCC HVDC converter. The upper part of the bridge legs can be seen as a maximum selector, just as the lower part can be understood as a minimum selector. According to this, the voltage seen from the DC side is the maximal line-to-line voltage, whichever it is at any instant. Figure illustrates this effect.

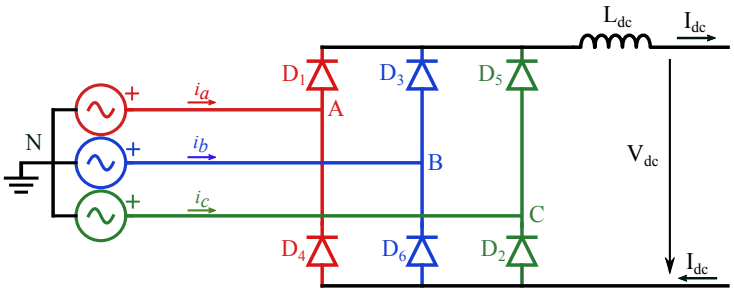

Figure 2.2: Ideal three-phase diode bridge

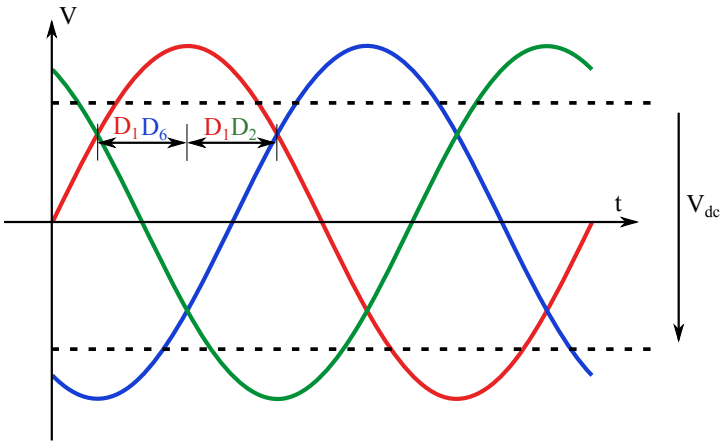

Figure 2.3: Waveforms and DC average voltage level for an ideal diode bridge

As it can be seen, each phase takes the maximum value for 120° periods, and the same can be said about the minimum value, albeit shifted 60°. Consequently, each 360° period can be divided into 60° intervals, in which there is a determinate maximum and minim phase voltage, thereby defining the converted line-to-line voltage waveform.

During the first marked interval, $V_{an}(t)$ is the maximal positive voltage, and $V_{bn}(t)$ is the minimal

voltage. Consequently, the conducting voltage will be $V_{ab}(t)$ during this interval, which corresponds to the diodes D1 and D6 conducting. After 60°, $V_{an}(t)$ remains the maximal voltage, however $V_{cn}(t)$ has become the minimal one. Therefore, D6 ceases to conduct and D2 starts conducting, making $V_{ac}(t)$ the voltage seen from the DC side, during this interval.

2.4 Three-phase thyristor bridge

Replacing diodes with thyristors, the working principle remains the same, however the turn-on time can be controlled by means of sending a pulse to the gate terminal of the thyristors. Ideally, if the pulse were to be sent at the start of each conducting interval (α=0), the thyristor bridge would behave exactly as a diode bridge.

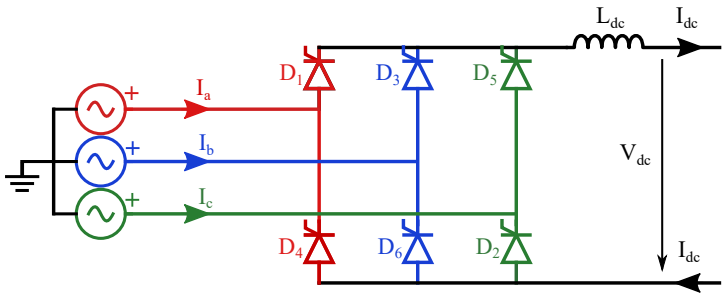

Figure 2.4: Three-phase thyristor bridge connected to an ideal AC voltage source

Delaying the turn-on of the thyristor offers controllability on the obtained DC voltage. The DC voltage can be directly controlled by the phase angle, depending also on the value of the line-to-line voltage (V_{LL}), as seen in the following equation:

$$V_{dc} = \frac{3\sqrt{2}}{\pi} V_{LL} \cos\alpha \simeq 1.35 V_{LL} \cos\alpha \tag{2.1}$$

Nevertheless, the underlying assumption on the precedent equation is that the commutation process from one valve to another is instantaneous. Once we consider a finite AC inductance L, the di/dt is limited up to a certain value, thus making the commutation process take significant amount of time, which is referred as the commutation angle μ (typically around 10° [5]). This angle is calculated as:

$$\mu = \arccos\left(\cos(\alpha) - \frac{I_{dc} 2\omega L}{\sqrt{2} V_{LL}}\right) - \alpha \tag{2.2}$$

This commutation angle has two principal effects on the HVDC converter:

- Reduces the mean DC voltage by the following amount:

$$\Delta V_{dc} = 3\frac{\omega L}{\pi} I_{dc} \tag{2.3}$$

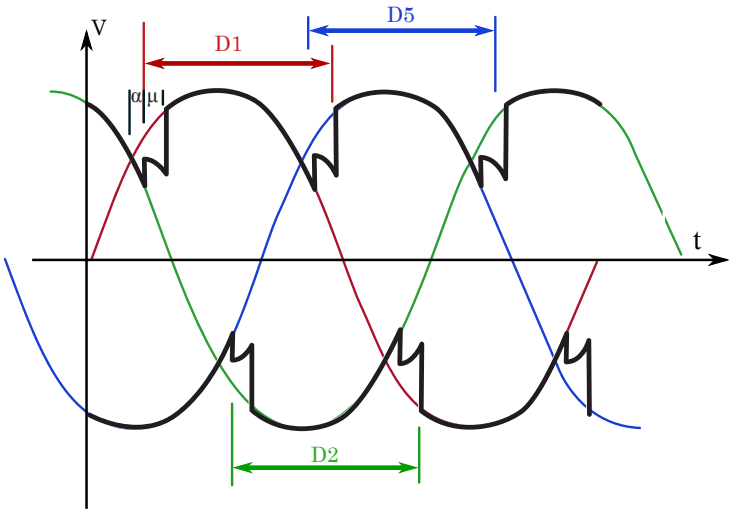

Figure 2.5: Effect of firing angle and commutation angle

- Imposes a practical limit on the value of the delay angle, as the commutation process cannot be extended beyond 180° without the risk of a commutation failure.

By increasing the delay angle beyond approximatively 90°, the voltage area of the DC terminals via the conducting thyristors will be predominantly negative, hence the DC terminal voltage will become negative, which corresponds with inverter operation. During inverter operation, it is more common to refer to the extinction angle γ than to the delay angle. Note that the definition of the extinction angle accounts for the commutation angle, as defined by:

$$\gamma = 180 - \alpha - \mu \tag{2.4}$$

Hence, for theoretical safe operation, the delay angle can go from 0 to $180-\mu$ (that is from $\alpha = 0$ to $\gamma = 0$). However, in order to assure a minimum voltage during the commutation process, there is practical minimal value for the delay angle (around 5°). Furthermore, in order to cover for any miscalculations or variations of the commutation angle, the extinction angle must be kept above 0.

2.4.1 AC and DC harmonic generation

Under normal conditions, 6-pulse converter harmonics are of order $n = 6k \pm 1$, whereas 12-pulse converter group generate current harmonies of order $n = 12k \pm 1$. That is because of the star-delta arrangement with a phase shift of 30°, which effectively cancels out some of the characteristic harmonics of a 6-pulse converter [5]. This is explained by the following principle:

- The AC current for a 6-pulse converter bridge connected through a YY transformer can be expressed as:

$$\Delta I_g = 2\frac{\sqrt{3}I_{dc}}{\pi}\left[\sin(\omega t) - \frac{1}{5}\sin(5\omega t) + \frac{1}{7}\sin(7\omega t) - \frac{1}{11}\sin(11\omega t) + \frac{1}{13}\sin(13\omega t)...\right] \tag{2.5}$$

Indicating that 6-pulse converters cause effectively current harmonics of order $n = 6k \pm 1$.

- On the other hand, the AC current generated by a 6-pulse converter bridge connected through a $Y\Delta$ transformer is given by:

$$\Delta I_g = 2\frac{\sqrt{3}I_{dc}}{\pi}\left[\sin(\omega t) + \frac{1}{5}\sin(5\omega t) - \frac{1}{7}\sin(7\omega t) - \frac{1}{11}\sin(11\omega t) + \frac{1}{13}\sin(13\omega t)...\right] \quad (2.6)$$

  Note how the $Y\Delta$ causes a phase shift of 180° in the 5^th, 7^th harmonics and multiples.

- Therefore, by combining two 6-pulse converter in those transformer arrangements, the global harmonic content can be theoretically reduced from a 37% THD (Total Harmonic Distortion) to a 13% [11].

Regarding DC harmonics, 12-pulse converters produce DC current harmonics of order $n = 12k$ while a single 6-pulse converter produces harmonics of order $n = 6k$. Moreover, the magnitude of the harmonics is reduced in a 12-pulse arrangement, thereby reducing DC current and voltage ripple.

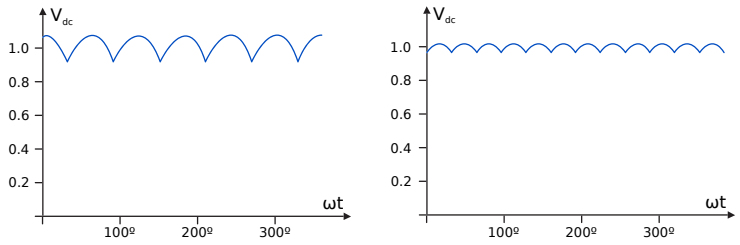

Figure 2.6: Comparison of the obtained DC voltage between a 6-pulse (a) and a 12-pulse (b) arrangement.

2.4.2 Reactive power

Neglecting the commutation angle, the power factor of the transformer can be approximated by $\cos(\alpha)$ (or $\cos(\gamma)$ in inverter mode), thus reactive power consumed increases as the delay angle approaches 90°. If we consider the commutation process, the reactive power absorption of a converter is approximated as:

$$Q_{dc,p.u.} = \tan\left(\arccos\left(\cos(\alpha,\gamma) - \frac{X_{ac}}{2}\right)\right) \quad (2.7)$$

A typical value for Q is 0.5 [1] at maximum rated power. Note that the power angle is given by:

$$\varphi = \arccos\left(\frac{\cos(\alpha)}{2} + \frac{\cos(\alpha+\mu)}{2}\right) \quad (2.8)$$

Chapter 3

LCC static characteristics

3.1 Introduction

This section presents the static curves of the LCC transmission system, which consists in the most important concept to understand the behaviour of an LCC-HVDC transmission system. Additionally, the static curves allow a first intuitive glimpse on the dynamics of this system.

3.2 Basic converter static characteristic

The control mode of the converters depends on the AC and DC prevailing conditions. The various steady-state modes are referred to as the static characteristics.

Figure 3.1 shows the steady-state model of the converter seen from its DC terminal. The purpose of the resistor is to represent the voltage drop caused by the converter bridge (related to the commutation process and the grid reactance X), although it bears no resistive losses. The DC voltage output represents the mean voltage level at the DC side of the converter bridge.

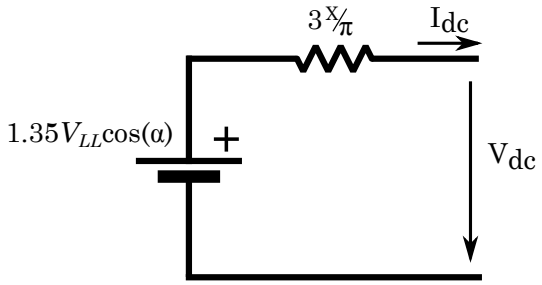

Figure 3.1: Equivalent steady-state model of the LCC converter from the DC outer terminal.

For a given delay angle, as the current approaches 1.0 p.u., the voltage drop increases reducing the DC voltage output of the converter. This relationship determines the natural V-I curve of

the converter. However, as the steady-state current cannot be above the rated value, a constant current control is imposed once the current reaches 1.0 p.u.. Those conditions yield the basic operating profile:

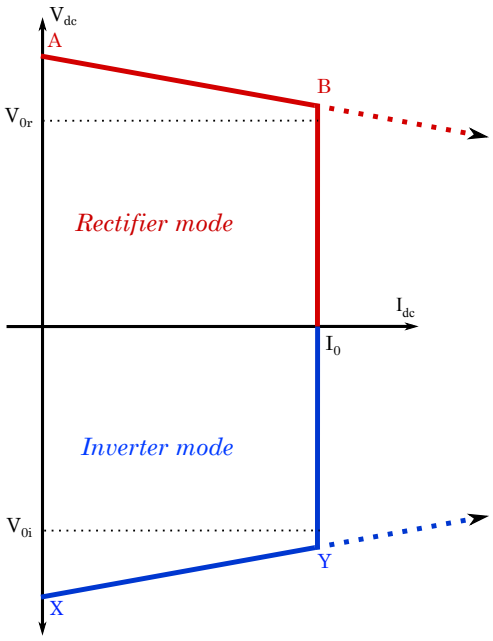

Figure 3.2: Equivalent steady-state model of the LCC converter from the DC outer terminal.

- The AB curve corresponds to the minimum delay angle control, known as Alfamin mode. The delay angle is kept at a constant minim value for as long as the current is below the rated value. Typical values for minimum delay angle go from 3° to 5° [1]. The slope depends on the AC voltage conditions and the grid reactance, defined by the following equation:

$$V_{dc} = 1.35 V_{LL} \cos(\alpha) - 3\frac{X}{\pi} I_{dc} \tag{3.1}$$

- The BY curve corresponds to the constant current mode, or current control mode. The current is kept at a constant desired value, which does not necessarily correspond to the maximum rated DC current, but can be set as desired. A controller will determine the appropriate delay angle in order to keep the current at the reference value. Once the voltage is reversed, roughly around a delay angle of 90°, the converter operates as an inverter.

- The XY curve corresponds to Constant Extinction Angle control (CEA). The extinction angle is kept as a minim value, typically around 10° to 15° [1]. In order to keep a constant γ, there is the need for an algorithm measuring the value of μ. The slope of the curve is given by:

$$V_{dc} = -1.35 V_{LL} \cos(\gamma) + 3\frac{X}{\pi} I_{dc} \tag{3.2}$$

Basic operation of a 2-terminal LCC system can be achieved with those control modes. By placing the rectifier and the inverter static characteristics on the same scheme, the operating points of the DC transmission are obtained. The following figure shows the static characteristic of this 2-terminal system, employing uniquely current control mode or constant angle mode (Alfamin/CEA):

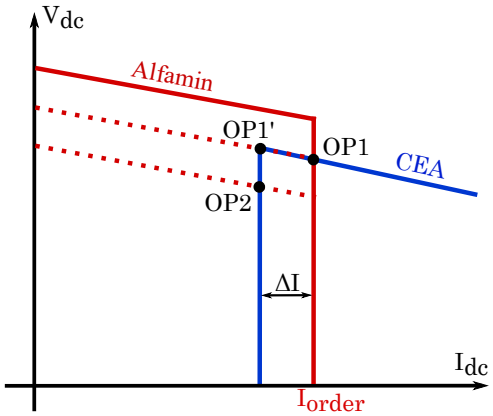

Figure 3.3: Basic static characteristic of an LCC-HVDC transmission.

In order to reach a stable operation point, the following strategy is employed: an outer power loop determines the current order for the rectifier, while the current order for the inverter is the rectifier current order minus the current margin (around 0.1 p.u. [1]). This forces the transmission system to reach a stable operation point OP1, in which the rectifier operates in current control mode (thus indirectly controlling the active power) and the inverter operates in constant extinction angle mode.

A reduction in the DC voltage of the rectifier (e.g. caused by a voltage sag on the AC side of the rectifier) displaces the operating point to OP2. In this case, the rectifier switches to Alfamin mode and the rectifier changes to current control mode. On the other hand, reduction of AC voltage on the inverter side would simply displace the operating point downward with lower DC voltage, without changing the control modes. In order to regain the rated DC power, the outer power loop will change the rectifier current order.

However, the robustness of this basic static characteristic is quite precarious. Operation at low DC voltage is far from ideal and there are no fault-management characteristics. Moreover, due to the slopes of the Alfamin and CEA modes, OP1′ is a dangerous operation point. From the standard operational point OP1, a small reduction in the rectifier AC voltage will bring closer the Alfamin and CEA curves, but the operation point stays at OP1. Then, a very small rectifier AC voltage reduction will displace the operating point moves to OP1′. Then, a very small rectifier AC voltage increase will cause the operating point to move back to OP1. Similar AC voltage changes in the inverter terminal will cause moves between OP1 and OP1′.

Furthermore, going back from OP1′ to OP1 implies an increase of DC current, which makes the converter draw more reactive power, i.e. reduces the AC voltage, thus displacing the point back to OP1. Then, thanks to the current decrease by moving to OP1′, the consumed reactive power

will go down, provoking a rise the AC voltage, and causing the operating point to bounce back to OP1. This is a highly undesirable phenomenon giving rise to power oscillations in both the AC and DC systems. This phenomenon as well as the lack of proper control modes in low DC voltage conditions justifies the need to expand the static characteristics beyond the basic control modes.

The following section will describe the typical static characteristics of a transmission scheme, expanding from the basic scheme shown in this section. Despite the improvements, the working principle will remain the same.

3.3 Typical LCC-HVDC transmission scheme static characteristics

The following figure shows the typical static characteristics of an LCC HVDC transmission. For sake of clarity constant Q curves have not been drawn on the diagram, however it is sufficient to know that Q is higher as the current rises and the voltage decreases. That is, in this scheme, the reactive power increases going from the top-left to bottom-right.

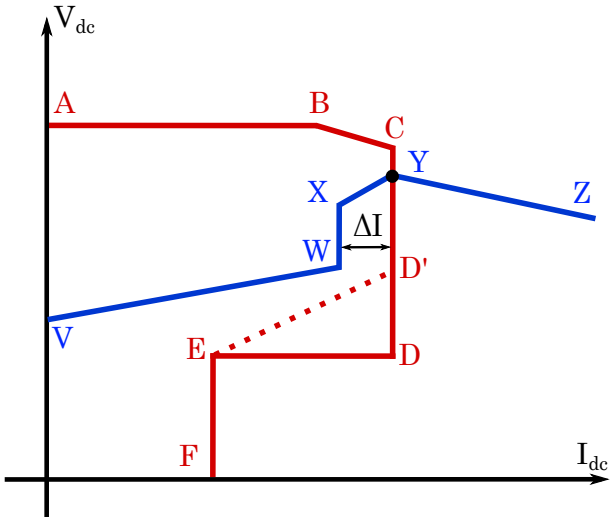

Figure 3.4: Typical static characteristic of an LCC-HVDC transmission.

- AB curve corresponds to constant DC voltage, which is use to limit the DC voltage should it raise above the threshold value. It is common used for open circuit testing in transmission schemes, but also to prevent DC overvoltage. It is typically set to 1.05 p.u.;
- BC is the Alfamin characteristic as referred in the previous section, commonly set around 3°-5°;
- CD corresponds to the constant current control mode, as referred in the previous section;

- DEF is the Low Voltage Current Clamp characteristic (LVCC), which is invoked only if the DC voltage falls below a preset level around 0.3 p.u. as a result of AC system fault or DC ground faults.
- D′E corresponds to a variation of the LVCC, which is defined as the Low Voltage Current Order Limiter (LVCOL). It is intended to reduce reactive power consumption during faults in the AC system.
- VW is the voltage dependent current limit. It is a current control mode with a reduced current order according to the voltage level. Typically, it goes from a DC voltage of 0.4 to 0.6 p.u. [1].
- WX corresponds to the constant current control mode, as referred in the previous section. The current reference is the same as the inverter, minus the current margin (typically 10%);
- XY is an adapted extinction angle control, in order to avoid the potential instabilities due to multiple operating points, as exposed in the last part of the previous section. This mode is called Betamax. In fact, it is the standard operating mode of the inverter, and it corresponds to a constant firing angle for the inverter.
- YZ corresponds to CEA mode, limiting the extinction angle at a predefined value, typically around 10°-20°.

This static characteristic is scheme-dependent, and has been built around the concept where the rectifier acts as a master (containing the outer power loop) and the inverter as a slave. Furthermore, for several cases, these characteristics may not be suitable. For example, the typical operating point corresponds to the inverter in Betamax and the rectifier in current control. However, other control strategies are possible. For example, when sending power to a power island, the standard approach may not be appropriate, as the response to sudden changes in power demand would not be fast enough, leading to possible frequency instabilities in the AC side of the inverter. For that case, it is better to change the static characteristics such as to force the standard inverter operating point in current control mode while maintaining the rectifier in CEA or Betamax mode, as this achieves a much faster response to power changes in the inverter side.

Chapter 4

LCC-HVDC operation

4.1 Introduction

Once the previous section has presented the static characteristics related to current and voltage, it is time to introduce the related static behaviour of active and reactive power. In fact, active and reactive power behaviour is strongly related to the stability of the transmission system. This chapter can be understood as a necessary preamble to the dynamic modelling of the LCC-HVDC transmission system.

4.2 Reactive and active power characteristic curves

The relationship (p.u.) between the reactive power absorbed and the AC and DC parameters is given by the following equations:

$$Q = I_{dc}\sqrt{k^2 V_{LL}^2 - V_{dc}^2} \tag{4.1}$$

$$k = \frac{V_{dc,0}}{V_{LL,0}\left(\cos(\alpha_0) - \frac{X}{2} I_{dc,0}\right)} \tag{4.2}$$

By substituting the values for DC current and voltage for a given scheme, the constant reactive power lines can be generated and placed on the static characteristics. On the other hand, constant active power curves can be obtained according to V/I characteristics.

For the sake of simplicity, only the basic static characteristics have been plotted in the previous figure. In practically all AC systems, AC source impedance is inductive at fundamental frequency. Therefore, assuming the AC system impedance as a simple inductor, constant reactive power lines can also be viewed as constant AC voltage lines.

4.3 Effects of AC voltage on converter operation

Both the DC voltage corresponding to the minim firing angle and minimum extinction angle are determined by the magnitude of the AC terminal voltage of the respective converters. Therefore,

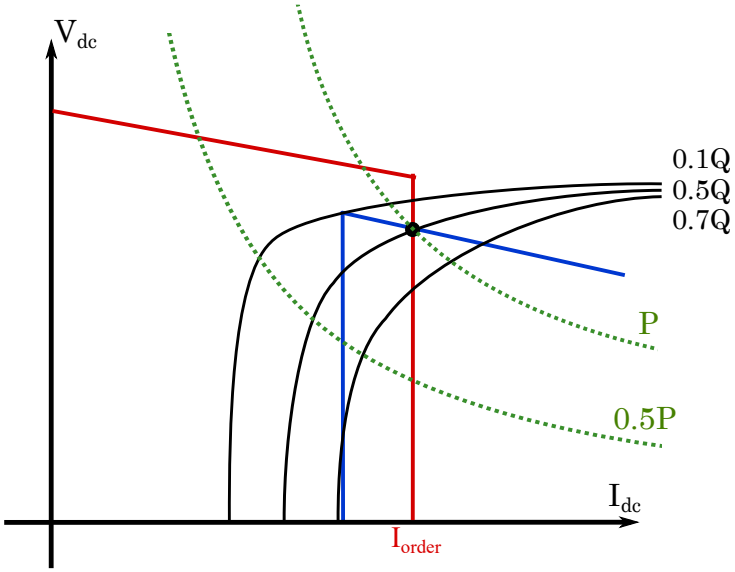

Figure 4.1: Steady-state constant active power and reactive power curves for an LCC transmission system

the positon of the V/I static characteristics of each converter is affected by the AC voltage at each terminal. Moreover, the AC voltage modifies the ordinate at origin of each of the characteristic curves, as the produced DC voltage is proportional to the AC terminal voltage.

A consequence of the operation of the converters, as seen in section 2.4, is the flow of reactive current from the AC system to the converters. This reactive current creates an voltage drop between the AC system voltage level and the converter busbar. Changing the converter AC terminal voltage directly interacts with the operating condition and vice-versa. The following sub-sections analyze this interaction effect for each of the converters.

4.3.1 Effects of sending end (rectifier) AC voltage fluctuations on system operation

This section discusses the effect of fluctuations of the rectifier AC terminal voltage on the system operation, i.e. it explains how changes in the prevailing AC conditions propagate through the transmission system.

Modifications of the operating point due to reductions of the AC rectifier voltage have already been discussed, pointing out the danger of a constant switching of operation points (c.f. section 3.2). A further consideration is the effect of the AC voltage reduction on the operation of the inverter. At first glance, equation 4.1 suggests the inverter reactive power consumption should be also reduced. However, as the reactive power compensated by capacitor banks depends on the square of the AC voltage, the net effect is an important increase in the consumed reactive power, causing the AC rectifier terminal voltage to fall further. This is a positive feedback relation and, particularly with weak AC systems, can lead to instabilities and eventual collapse

of the sending end AC system voltage.

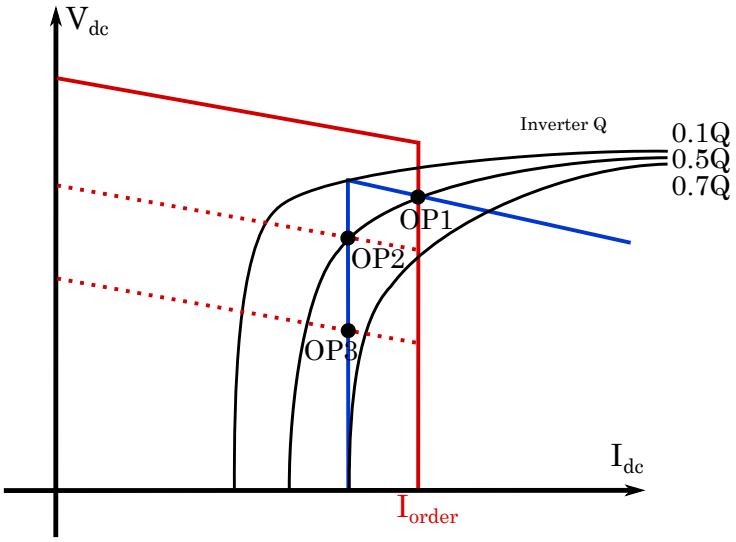

Figure 4.2: Inverter reactive power curves

However, the effect of inverter reactive power and its interaction between the reduction of AC voltage has not been discussed so far. In fact, as the AC system voltage falls down, the operational point sweeps through increasing reactive power lines. That is, the reduction of the rectifier AC voltage causes a shift of the operational point, translating in higher reactive power consumption at the inverter. If the inverter is connected to a relatively strong AC system, i.e. there is a very low impedance between the converter and the ideal AC voltage source, then the increase in reactive power consumption will be of little consequence. However, if the inverter AC connection system is weak, the increased reactive power consumption of the inverter will result in the inverter voltage being furtherly reduced. In extreme cases, an AC fault near the AC terminal of the rectifier will result in significant and inadmissible reductions of the inverter terminal voltage. This means that the fault at the sending AC system will be exported to the receiving AC system and will adversely affect it. This relationship between converter operation and terminal voltage gives rise to possible interactions and possible instabilities.

4.3.2 Effects of the receiving end (inverter) AC voltage fluctuations on system operation

Reductions of the AC voltage at the inverter terminal voltage also have an effect on the inverter itself and on the rectifier. On one hand, the operating point will move down the rectifier constant current characteristic as seen in the following figure. A consequence of moving the operating point down is an increased reactive power consumption at the inverter, and if the AC system at the inverter terminal is particularly weak, this will depress the rectifier AC system voltage.

As in the previous section, the reduction if the inverter AC voltage will reduce the inverter reactive power consumption, but the reactive power support from filters and capacitors will be

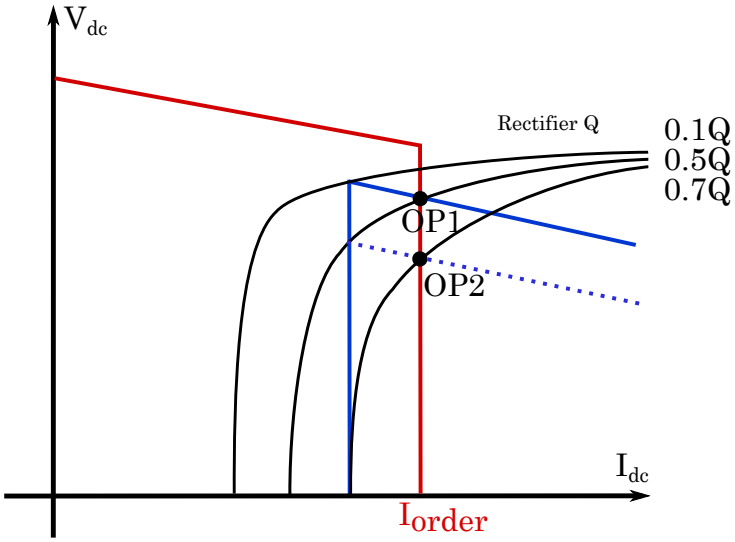

Figure 4.3: Inverter reactive power curves

reduced more significantly. Therefore, the effective reactive power consumption will increase furtherly decreasing the inverter AC voltage. This is again a positive feedback condition, which can lead to the collapse of the AC inverter voltage resulting on the loss of all power transmission.

4.4 Indicators related to AC/DC interactions

In the previous sections, it has been emphasized that the magnitude of the AC/DC interactions is strongly related with the strength of the AC grid. Consequently, this subsection will analyse the AC/DC interaction for various grid strengths, from a power system point of view.

4.4.1 Indicators for grid strength with a single HVDC connection

Several indicators attempting to measure grid strength can be found in the literature. Note that all of them relate to the strength of the AC grid relative to the DC link. That is, the indicators do not measure the absolute strength of the AC grid, but a value relative to the connected DC power.

As mentioned earlier, the strength of an AC grid can be related to the short-circuit apparent power (S_{sc}) at a particular bus. In fact, given the AC line-to-line voltage level, the equivalent AC system impedance is calculated as $Z_{eq} = \frac{V_0}{Z_{eq}}$, where V_0 is the no-load line-to-line voltage level.

Although this equivalent impedance is sometimes assumed to be purely inductive (at fundamental frequency), a slightly more accurate approach is to consider an R-L impedance, albeit generally with a phase angle close to 90°. Moreover, the phase angle θ of the impedance is calculated from the X/R ratio of the AC system:

$$\theta = \arctan\left(\frac{X}{R}\right) \tag{4.3}$$

A typical value of the X/R ratio for AC transmission systems is 10, which yields a phase angle of 84.3°. Regarding AC-DC connections, the relative strength is evaluated by the short-circuit ratio (SCR), given by:

$$SCR = \frac{S_{sc}}{P_{dc}} \tag{4.4}$$

The SCR has a direct relation with the voltage fluctuations between the AC ideal source and the converter AC voltage. A strong AC system is defined as one with a SCR greater than 3, while a weak AC system corresponds to an SCR between 2 and 3. However, this relationship ignores the impact of local shunt-connected capacitor banks. In order to take the local capacitor banks into account, the SCR must be modified, giving the equivalent short-circuit ratio (ESCR), which is defined as:

$$ESCR = \frac{S_{sc} - Q_{bank}}{P_{dc}} \tag{4.5}$$

Beyond a certain level of AC power transmission, any further increase in the DC current for CEA will result in a reduction of the converter AC terminal voltage, hence reducing the transmitted DC power. For a given AC system, the maximum DC power that can be transmitted before the AC voltage level falls can be defined as the Critical Equivalent Short-Circuit Ratio (CESCR). The equation for CESCR assumes the AC system to be purely inductive, and is given in p.u. by:

$$CESCR = \frac{P_{dc}\cot\left(\frac{90 - \gamma - \mu}{2}\right) - Q_{converter}}{V_{ac}^2} \tag{4.6}$$

4.4.2 Maximum power curve

In order to understand the effect of SCR (or ESCR) and its relationship with AC/DC interactions, the maximum power curve serves as an excellent tool. By plotting the AC transmitted power as well as the AC voltage as a function of DC current, the influence of the SCR is revealed.

As the SCR is increased, the profile of the P_{ac}-I_{DC} curve is modified. For a high SCR, the profile is monotonous, resemblant to a identity curve as the SCR increases. However, for lower SCR, the point of Maximum Available Power (MAP) is displaced to increasingly lower DC current. Note that for an SCR of 2.0, the MAP is reached at a DC current of 1.0 p.u., representing the lower SCR threshold for stability (although this bears no margin for disturbances). For smaller SCRs (e.g. 1.5), it can be seen that the MAP (i.e. the stability limit) lays at DC currents lower than the rated one, making operation at full rated power impossible. In practice, with very weak AC systems, nor pure CEA control nor Betamax is recommended, instead other control

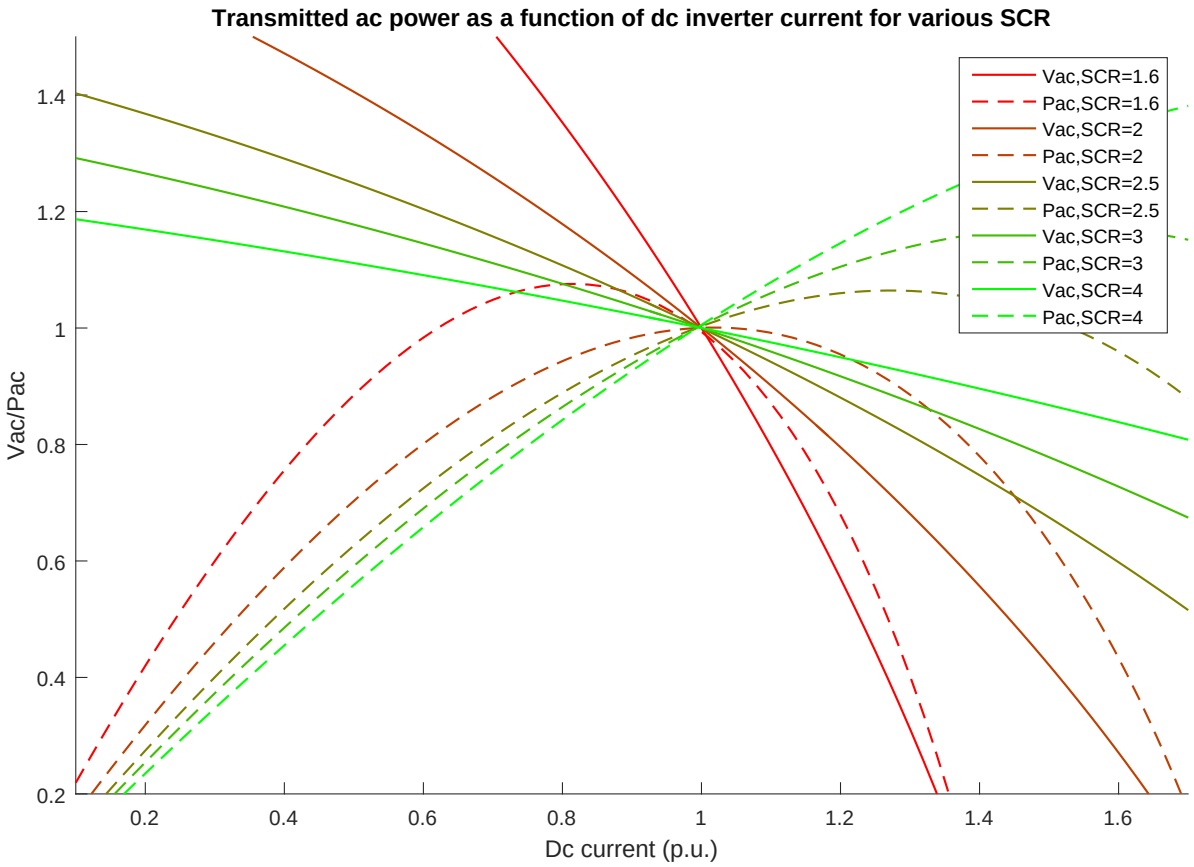

Figure 4.4: Transmitted AC power as a function of DC inverter current for various SCR

techniques are used which can provide some feedback in terms of the converter station response to AC voltage reductions. Therefore, SCRs lower than two are achievable in standard conditions.

On the other hand, while probably no one would employ CEA in a weak AC-DC interconnections, it is quite possible that a contingency on the AC side of the system (e.g., the loss of a line or nearby generator) causes a normally strong SCR to fall below a value of 3.

4.5 Summary

The studied steady-state behaviour allows to anticipate on the most problematic characteristics of the LCC converter regarding stability and the small-signal model: the relationship between the inner state of the converter and the consumed AC reactive power, and more particularly the effect of the commutation angle on the ac-side reactive power, which can transmit undesired dynamics from the DC-side to the AC-side.

Chapter 5

LCC-HVDC link small-signal modelling

5.1 Introduction

This section discloses the construction of an LCC small-signal model of a 6-pulse LCC-HVDC transmission system. There is a simpler model and a complete one. The first and basic small-signal model is considered an introduction to the basic systems that must be modelled. With respect to the basic model, the complete small-signal model includes controller dynamics and AC system dynamics, as well as the effect of commutation angle.

5.2 HVDC small-signal model

5.2.1 DC-side model

The first step is to obtain the state space model of the DC system, made up by the DC cables and DC reactors. The following figure shows a schematic of the DC system.

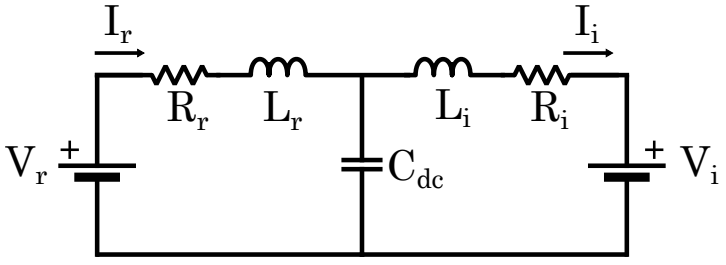

Figure 5.1: DC system model

The following variable are defined as:

- I_r: DC current through rectifier DC terminals;

- I_i: DC current through inverter DC terminals;
- V_{dc}: DC voltage at the cable midpoint;
- L_r, R_r : Inductance and resistance of the rectifier DC system;
- L_i, R_i : Inductance and resistance of the inverter DC system;
- C_{dc} : Capacitance of the DC cables;
- V_r : DC terminal rectifier voltage;
- V_i : DC terminal inverter voltage.

Note that the DC parameters are given by the DC smoothing reactors as well as the cable lumped parameters. The DC terminal voltage of both converters is a controlled magnitude (by means of angles α or γ). The systems yields the following dynamic equations:

$$\begin{pmatrix} V_r = I_r(R_r + sL_r) + V_{dc} \\ V_i = -I_i(R_i + sL_i) + V_{dc} \\ sC_{dc}V_{dc} = I_r - I_i \end{pmatrix} \tag{5.1}$$

The state controlled variables being the DC voltage level at the converters, the previous equations can be arranged in the following way:

$$\begin{bmatrix} \dot{I}_r \\ \dot{I}_i \\ \dot{V}_{dc} \end{bmatrix} = \begin{bmatrix} \frac{-R_r}{L_r} & 0 & \frac{-1}{L_r} \\ 0 & \frac{-R_i}{L_i} & \frac{+1}{L_i} \\ \frac{1}{C_{dc}} & \frac{-1}{C_{dc}} & 0 \end{bmatrix} \begin{bmatrix} I_r \\ I_i \\ V_{dc} \end{bmatrix} + \begin{bmatrix} \frac{1}{L_r} & 0 \\ 0 & \frac{-1}{L_i} \\ 0 & 0 \end{bmatrix} \begin{bmatrix} V_r \\ V_i \end{bmatrix} \tag{5.2}$$

All the parameters appearing in the equations can be obtained with a high degree of precision (as they are design variables) save the cable capacitance, which should be given by the cable supplier.

5.2.2 HVDC line-commutated converter

The goal of this subsection is to replace the previous control variables V_r and V_i with an expression that incorporates the behaviour of the converter. The previous DC system equations must be therefore expanded by the converter equations, given by:

$$V_r = \frac{3\sqrt{2}}{\pi} V_{LL,r} \cos(\alpha_r) - 3\frac{\omega_r L_{ac,r}}{\pi} I_r \tag{5.3}$$

$$V_i = \frac{-3\sqrt{2}}{\pi} V_{LL,i} \cos(\alpha_i) + 3\frac{\omega_i L_{ac,i}}{\pi} I_i \tag{5.4}$$

Where:

- L_{ac} is the equivalent inductance for each of the converter AC terminals (the grid equivalent impedance is assumed to be purely inductive);

- V_{LL} is the line-to-line voltage level at each of the converter AC terminals.

The sign inversion in the inverter equations corresponds to the disposition of this converter. Note that this expressions are non linear and must be linearised in order to be included in the state-space small-signal model. Regarding the linearisation, the following assumptions are made:

- The AC frequency on both terminals is assumed to be constant
- The equivalent inductance on both terminals is also assumed to be constant.

Thus, there are three variables subjected to the small signal analysis, which are to be accounted for as non-null derivatives. Additionally, the variables are replaced by its incremental expressions. Consequently, the following equations are obtained:

$$\Delta V_{dc,r} \simeq \frac{-3\sqrt{2}}{\pi} V_{LL0,r} \sin(\alpha_r)\Delta\alpha_{r0} + \frac{3\sqrt{2}}{\pi}\cos(\alpha_{r0})\Delta V_{LL,r} - 3\frac{\omega_r L_{ac,r}}{\pi}\Delta I_r \tag{5.5}$$

$$\Delta V_{dc,i} \simeq \frac{3\sqrt{2}}{\pi} V_{LL0,i} \sin(\alpha_{i0})\Delta\alpha_{i} + \frac{-3\sqrt{2}}{\pi}\cos(\alpha_{i0})\Delta V_{LL,i} + 3\frac{\omega_i L_{ac,i}}{\pi}\Delta I_i \tag{5.6}$$

The zero subscripts correspond to the linearisation point. Then, the equations are merged with the previous state-space model, which yields:

$$\begin{bmatrix} \dot{I}_r \\ \dot{I}_i \\ \dot{V}_{dc} \end{bmatrix} = \begin{bmatrix} \frac{-R_r}{L_r} - \frac{3\omega_r L_{ac,r}}{\pi L_r} & 0 & \frac{-1}{L_r} \\ 0 & \frac{-R_i}{L_i} - \frac{3\omega_r L_{ac,i}}{\pi L_i} & \frac{+1}{L_i} \\ \frac{1}{C_{dc}} & \frac{-1}{C_{dc}} & 0 \end{bmatrix} \begin{bmatrix} I_r \\ I_i \\ V_{dc} \end{bmatrix} + \begin{bmatrix} \frac{3\sqrt{2}\cos(\alpha_{r0})}{\pi L_r} & 0 & \frac{-3\sqrt{2}V_{LL0,r}\sin(\alpha_{r0})}{\pi L_r} & 0 \\ 0 & \frac{-3\sqrt{2}\cos(\alpha_{i0})}{\pi L_i} & 0 & \frac{3\sqrt{2}V_{LL0,i}\sin(\alpha_{i0})}{\pi L_i} \\ 0 & 0 & 0 & 0 \end{bmatrix} \begin{bmatrix} \Delta V_{LL,r} \\ \Delta V_{LL,i} \\ \Delta\alpha_r \\ \Delta\alpha_i \end{bmatrix} \tag{5.7}$$

Note that the state matrix is not dependent on the linearisation point, being valid for any system conditions. However, the input matrix is heavily dependent on the linearisation point; even the sign of its terms is depending on the system conditions, due to the presence of trigonometric functions.

While the system is characterized by its previously built state equation, an output equation is needed in order to tune the controllers in the next subsection. For this reason, it is natural to choose the output variables as the voltage levels of the DC terminals, as well as the state variables.

5.3 Complete HVDC and HVAC small-signal model

5.3.1 HVDC system

This system is characterized in a very similar manner as in (5.7). The modification comes from separating the AC line-to-line voltage level in its qd components (c.f. Appendix C). The number

of input variables is expanded to 6, re-defining the state equation. For the sake of simplicity, some constants have been defined at the state-space representation. Those constants are defined at the end of this subsection.

$$\Delta V_{LL,r} \simeq K_{2r} \left(V_{qr0} \Delta V_{qr} + V_{dr0} \Delta V_{dr} \right) \tag{5.8}$$

$$\Delta V_{LL,i} \simeq K_{2i} \left(V_{qi0} \Delta V_{qi} + V_{di0} \Delta V_{di} \right) \tag{5.9}$$

By rearranging 5.7 with 5.8 and 5.9, the state-space representation of the HVDC system becomes:

$$\begin{bmatrix} \dot{I}_r \\ \dot{I}_i \\ \dot{V}_{dc} \end{bmatrix} = \begin{bmatrix} \frac{-R_r}{L_r} - \frac{3\omega_r L_{ac,r}}{\pi L_r} & 0 & \frac{-1}{L_r} \\ 0 & \frac{-R_i}{L_i} - \frac{3\omega_r L_{ac,i}}{\pi L_i} & \frac{+1}{L_i} \\ \frac{1}{C_{dc}} & \frac{-1}{C_{dc}} & 0 \end{bmatrix} \begin{bmatrix} I_r \\ I_i \\ V_{dc} \end{bmatrix} + \begin{bmatrix} \frac{K_{vr} K_{2r} V_{rq0}}{L_r} & \frac{K_{vr} K_{2r} V_{rd0}}{L_r} & 0 & 0 & \frac{-K_{1r}}{L_r} & 0 \\ 0 & 0 & \frac{K_{vi} K_{2i} V_{iq0}}{L_i} & \frac{K_{vi} K_{2i} V_{id0}}{L_i} & 0 & \frac{-K_{1i}}{L_i} \\ 0 & 0 & 0 & 0 & 0 & 0 \end{bmatrix} \begin{bmatrix} \Delta V_{rq0} \\ \Delta V_{rd0} \\ \Delta V_{iq0} \\ \Delta V_{id0} \\ \Delta \alpha_r \\ \Delta \alpha_i \end{bmatrix} \tag{5.10}$$

Regarding the definitive output equation, state variables as well as a set of other parameters are chosen. It is useful to output the DC voltage level of both converters as those will be used for calculating the active power exchanged at each converter. Moreover, the commutation angles μ_r and μ_i can be determined from the system state and control variables. Besides being relevant parameters, the commutation angle is needed to estimate the reactive power exchanged at the converters AC terminals. Consequently, the following equation is to be linearized:

$$\mu = \arccos \left(\cos \left(\alpha \right) - \frac{I_{dc} 2\omega L_{ac}}{\sqrt{2} V_{LL}} \right) - \alpha \tag{5.11}$$

$$\Delta \mu_r \simeq K_{\mu r} \sin \left(\alpha_{r0} \right) \Delta \alpha_r + \frac{K_{\mu r} K_{\mu r2}}{V_{LL0r}} \Delta I_r - \frac{K_{\mu r} K_{\mu r2} I_{r0}}{V_{LL0r}^2} K_{2r} V_{rq0} \Delta V_{rq} - \frac{K_{\mu r} K_{\mu r2} I_{r0}}{V_{LL0r}^2} K_{2r} V_{rd0} \Delta V_{rd} V_{rq} \tag{5.12}$$

Note that this equation may have a narrow linearisation range due to the involved functions. This would probably imply higher differences between the linearised model and the non-linear model when analysing variables issued from μ.

$$
\begin{bmatrix} \dot{I}_r \\ \dot{I}_i \\ \dot{V}_{dc} \end{bmatrix} = \begin{bmatrix} 1 & 0 & 0 \\ 0 & 1 & 0 \\ 0 & 0 & 1 \\ -\frac{3\omega_r L_{ac,r}}{\pi} & 0 & 0 \\ 0 & +\frac{3\omega_i L_{ac,i}}{\pi} & 0 \\ \frac{K_{\mu r} K_{\mu r 2}}{V_{LLr0}} & 0 & 0 \end{bmatrix} \begin{bmatrix} I_r \\ I_i \\ V_{dc} \end{bmatrix} + \begin{bmatrix} 0 & 0 & 0 & 0 & 0 & 0 \\ 0 & 0 & 0 & 0 & 0 & 0 \\ 0 & 0 & 0 & 0 & 0 & 0 \\ K_{vr} K_{2r} V_{rq0} & K_{vr} K_{2r} V_{rd0} & 0 & -K_{1r} & 0 & 0 \\ 0 & 0 & -K_{vi} K_{2i} V_{iq0} & -K_{vi} K_{2i} V_{id0} & 0 & -K_{1i} \\ \frac{-K_{\mu r} K_{\mu r 2} I_{dcr0} K_{2r} V_{rq0}}{V_{LLr0}^2} & \frac{-K_{\mu r} K_{\mu r 2} I_{dcr0} K_{2r} V_{rd0}}{V_{LLr0}^2} & 0 & 0 & K_{\mu r} \sin(\alpha_{r0}) - 1 & 0 \end{bmatrix} \begin{bmatrix} \Delta V_{rq0} \\ \Delta V_{rd0} \\ \Delta V_{iq0} \\ \Delta V_{id0} \\ \Delta \alpha_r \\ \Delta \alpha_i \end{bmatrix} \tag{5.13}
$$

This state-space system is the centrepiece of the whole model. As it will be shown in following sections, its outputs are feed to the AC system, which in turn feeds back some of its outputs as inputs of the HVDC state-space system (AC terminal voltage levels). Regading the constants, they are defined as follows:

$$K_{vr} = \frac{3\sqrt{2}}{\pi \cos(\alpha_{r0})} \tag{5.14}$$

$$K_{vi} = \frac{3\sqrt{2}}{\pi \cos(\alpha_{i0})} \tag{5.15}$$

$$K_{1r} = \frac{3\sqrt{2}}{\pi V_{LLr0} \sin(\alpha_{r0})} \tag{5.16}$$

$$K_{1i} = \frac{3\sqrt{2}}{\pi V_{LLr0} \sin(\alpha_{i0})} \tag{5.17}$$

$$K_{2r} = \frac{\sqrt{\frac{2}{3}}}{\sqrt{V_{rq0}^2 + V_{rd0}^2}} \tag{5.18}$$

$$K_{2i} = \frac{\sqrt{\frac{2}{3}}}{\sqrt{V_{iq0}^2 + V_{id0}^2}} \tag{5.19}$$

$$K_{rq} = I_{r0} \cos(\alpha_{r0}) \tag{5.20}$$

$$K_{rd} = I_{r0} \sin(\alpha_{r0}) \tag{5.21}$$

$$K_{\mu r2} = \frac{2\omega_r L_{ac}}{\sqrt{2}} \tag{5.22}$$

$$K_{\mu i2} = \frac{2\omega_i L_{ac}}{\sqrt{2}} \tag{5.23}$$

$$K_{\mu r} = \frac{1}{\sqrt{1 - \left(\cos(\alpha_{r0}) - \frac{I_{r0} K_{\mu r2}}{V_{LLr0}^2}\right)}} \tag{5.24}$$

$$K_{\mu i} = \frac{1}{\sqrt{1 - \left(\cos(\alpha_{i0}) - \frac{I_{i0} K_{\mu i2}}{V_{LLi0}^2}\right)}} \tag{5.25}$$

5.3.2 Control system

As the rectifier normally operates on constant current control, there is the need to incorporate the dynamics of this control. For this purpose, the equations of the tuned PI controller must be converter in the state-space representation. First of all, let us consider the control equations under the Laplacian form:

$$\alpha_r = \frac{K_p s + K_i}{s} \left(I_r^* - I_r\right) \tag{5.26}$$

Note that in order to build an equivalent state-space representation, it is necessary to define two state variables, which will be the integrals of I_r^* and I_r. This leaves a null state matrix and an indentity input matrix. The output equation corresponds to the output of the controller, which is α_r.

$$\frac{d}{dt}\begin{bmatrix} intI_r \\ intI_r^* \end{bmatrix} = \begin{bmatrix} 0 & 0 \\ 0 & 0 \end{bmatrix}\begin{bmatrix} intI_r^* \\ intI_r \end{bmatrix} + \begin{bmatrix} 1 & 0 \\ 0 & 1 \end{bmatrix}\begin{bmatrix} I_r^* \\ I_r \end{bmatrix} \tag{5.27}$$

$$\Delta\alpha_r = \begin{bmatrix} K_i & -K_i \end{bmatrix}\begin{bmatrix} intI_r^* \\ intI_r \end{bmatrix} + \begin{bmatrix} K_p & -K_p \end{bmatrix}\begin{bmatrix} I_r^* \\ I_r \end{bmatrix} \tag{5.28}$$

$$intI_r^* = \int I_r^* \tag{5.29}$$

$$intI_r = \int I_r \tag{5.30}$$

The output of this system is then fed back to the HVDC state-space system as an input, as seen in (5.10). Regarding the inverter, there is no need to have a dedicate small-signal model of the controllers, as in Betamax control the extinction angle α_i is kept constant.

5.3.3 AC-DC interface

In order to link the previous HVDC system to both AC-sides, it is necessary to define some functions that will express DC-magnitudes into AC-equivalents. The link between AC and DC systems is based on a PQ approach, which is to model the AC converter terminals such as to exchange the same power as the DC converter terminals. Reactive power is deduced thanks to the estimation of power angle φ provided by (2.8). Linearisation of this equation yields:

$$\Delta\varphi_r \simeq \left[\frac{\sin\left(\alpha_{r0}\right)}{2\sin\left(\varphi_{r0}\right)} + \frac{\sin\left(\alpha_{r0}+\mu_{r0}\right)}{2\sin\left(\varphi_{r0}\right)}\right]\Delta\alpha_r + \frac{\sin\left(\alpha_{r0}+\mu_{r0}\right)}{2\sin\left(\varphi_{r0}\right)}\Delta\mu_r \tag{5.31}$$

$$\Delta\varphi_i \simeq \left[\frac{\sin\left(\alpha_{i0}\right)}{2\sin\left(\varphi_{i0}\right)} + \frac{\sin\left(\alpha_{i0}+\mu_{i0}\right)}{2\sin\left(\varphi_{i0}\right)}\right]\Delta\alpha_i + \frac{\sin\left(\alpha_{i0}+\mu_{i0}\right)}{2\sin\left(\varphi_{i0}\right)}\Delta\mu_i \tag{5.32}$$

Note that equations 5.31 and 5.32 are purely algebraic and therefore can be represented by a constant gain, for a given linearisation point. On the other hand, active power is calculated at

the DC terminals of each converter, and reactive power is estimated from the active power and the power factor angle by:

$$\begin{aligned} P_r &= V_r I_r \\ Q_r &= P_r \tan(\varphi_r) \end{aligned} \tag{5.33}$$

$$\begin{aligned} P_i &= V_i I_i \\ Q_i &= P_i \tan(\varphi_i) \end{aligned} \tag{5.34}$$

Therefore, incremental values are given by:

$$\begin{aligned} \Delta P_r &= V_{r0}\Delta I_r + I_{r0}\Delta V_r \\ \Delta Q_r &= V_{r0}\tan(\varphi_{r0})\,\Delta I_r + I_{r0}\tan(\varphi_{r0})\,\Delta V_r + \tfrac{I_{r0}V_{r0}}{\cos^2(\varphi_{r0})}\Delta\varphi_r \end{aligned} \tag{5.35}$$

$$\begin{aligned} \Delta P_i &= V_{i0}\Delta I_i + I_{i0}\Delta V_i \\ \Delta Q_i &= V_{i0}\tan(\varphi_{i0})\,\Delta I_i + I_{i0}\tan(\varphi_{i0})\,\Delta V_i + \tfrac{I_{i0}V_{i0}}{\cos^2(\varphi_{i0})}\Delta\varphi_r \end{aligned} \tag{5.36}$$

Again, those are algebraic equation and treated as a linear gain. Once the equivalent active and reactive power at the converter AC terminals is calculated, the equivalent AC current is determined using pq theory [12]. Using the q-axis as the reference point, pq theory allows to calculate the q-d components of the current for a given voltage and power:

$$i_q = \frac{3}{2}\frac{V_q P - V_d Q}{V_q^2 + V_d^2} \tag{5.37}$$

$$i_d = \frac{3}{2}\frac{V_d P + V_q Q}{V_q^2 + V_d^2} \tag{5.38}$$

Linearising those equations yields the following algebraic equation:

$$\begin{aligned} \Delta i_q = \frac{3}{2}\Big(&\frac{V_{q0}}{V_{qo}^2 + V_{do}^2}\Delta P + \frac{-V_{d0}}{V_{qo}^2 + V_{do}^2}\Delta Q + \frac{\left(V_{qo}^2 + V_{do}^2\right)P_0 - 2V_{q0}\left(V_{q0}P_0 - V_{d0}Q_0\right)}{\left(V_{qo}^2 + V_{do}^2\right)^2}\Delta V_q \\ &+ \frac{-\left(V_{qo}^2 + V_{do}^2\right)Q_0 + 2V_{d0}\left(V_{q0}P_0 - V_{d0}Q_0\right)}{\left(V_{qo}^2 + V_{do}^2\right)^2}\Delta V_d\Big) \end{aligned} \tag{5.39}$$

$$\begin{aligned} \Delta i_q = \frac{3}{2}\Big(&\frac{V_{d0}}{V_{qo}^2 + V_{do}^2}\Delta P + \frac{V_{q0}}{V_{qo}^2 + V_{do}^2}\Delta Q + \frac{\left(V_{qo}^2 + V_{do}^2\right)Q_0 - 2V_{q0}\left(V_{d0}P_0 + V_{q0}Q_0\right)}{\left(V_{qo}^2 + V_{do}^2\right)^2}\Delta V_q \\ &+ \frac{\left(V_{qo}^2 + V_{do}^2\right)P_0 - 2V_{d0}\left(V_{d0}P_0 + V_{q0}Q_0\right)}{\left(V_{qo}^2 + V_{do}^2\right)^2}\Delta V_d\Big) \end{aligned} \tag{5.40}$$

Combining all of the previous equations, which are all algebraic (i.e. constant gains for a given linearisation point), the link between the DC system and both AC systems can be established. For sake of clarity, the r and i subscripts have not been added as the equations are difficult enough to read. Of course, these equations apply both to the recitfier and inverter variables.

5.3.4 AC grid model

The AC grid model is modelled as a Thevenin equivalent with a capacitor in parallel, the latter representing the capacitor banks. Note that these capacitor banks represented the reactive compensation from both the AC filters and the real capacitor banks. On the other hand, in order to employ a small-signal model, the linearisation of the AC grid must be done in the q-d framework. Note that there is no transformer inductance. As mentioned in [5], there is no need to consider it (and it would be incompatible with modelling the DC system as a current source) as it has been already taken in account in the converter equations 5.3 and 5.4 as a voltage drop. Then, the dynamic effect of the inductance is considered by adding it to the DC inductance.

The following figure shows the considered model of the AC grid, both for the rectifier and inverter.

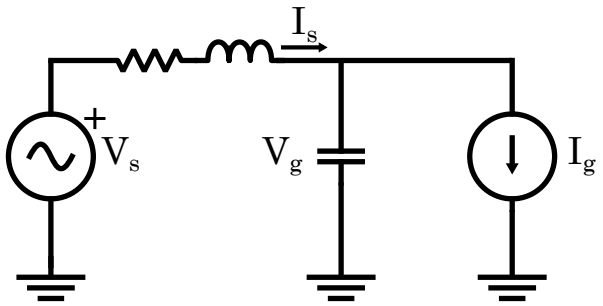

Figure 5.2: Modelled AC system including filter dynamics

The inputs of this model will be the voltage source (q and d component) and the equivalent current (q and d component, obtained as explained in the previous subsection) linking the AC system with the DC system. Its key output will be the voltage level at the converter AC terminals. Note that the equations are exactly the same for the rectifier and inverter equivalent AC grids, albeit the parameters may be different.

In order to modelize the AC grid, first of all the original ODEs describing the AC system in the abc frame must be considered:

$$V_{s,abc} - V_{g,abc} = r_s I_{s,abc} + l_s \frac{d}{dt} I_{s,abc} \tag{5.41}$$

$$C_{ac} \frac{d}{dt} V_{g,abc} = I_{s,abc} - I_{g,abc} \tag{5.42}$$

The current through the source inductance and the voltage across the AC capacitors are the obvious choices for state variables. Among the output variables must necessarily be the V_g voltage, as it corresponds to the voltage of the converters AC terminals and is used for various calculation in the HVDC system. Note that the above equations, in the abc frame, can't be directly used in a small-signal model, as those signals are constantly oscillating and do not correspond to constant values. However, if expressed in the q-d reference frame, 50 Hz signals are transformed in DC signals, thereby allowing to build a small-signal model. By applying Park's transformation to the above equations, the small-signal model in the q-d frame is obtained:

$$\begin{bmatrix} \dot{I}_{sq} \\ \dot{I}_{sd} \\ \dot{V}_{gq} \\ \dot{V}_{gd} \end{bmatrix} = \begin{bmatrix} \frac{-r_s}{l_s} & -\omega & \frac{-1}{l_s} & 0 \\ \omega & \frac{-r_s}{l_s} & 0 & \frac{-1}{l_s} \\ \frac{1}{C_{ac}} & 0 & 0 & -\omega \\ 0 & \frac{1}{C_{ac}} & -\omega & 0 \end{bmatrix} \begin{bmatrix} I_{sq} \\ I_{sd} \\ V_{gq} \\ V_{gd} \end{bmatrix} + \begin{bmatrix} 0 & 0 & \frac{1}{l_s} & 0 \\ 0 & 0 & 0 & \frac{1}{l_s} \\ \frac{-1}{C_{ac}} & 0 & 0 & 0 \\ 0 & \frac{-1}{C_{ac}} & 0 & 0 \end{bmatrix} \begin{bmatrix} I_{gq} \\ I_{gd} \\ V_{sq} \\ V_{sd} \end{bmatrix} \tag{5.43}$$

The output equation will simply be a mirror of the state variables, as they contain the q-d components of the converter AC votlage. That is, the output matrix is a fourth-order identity matrix and there is no feed-forward matrix. It should suffice with a null-expanded second-order identity matrix, but it is also interesting to be able to observe changes in all state variables.

$$\begin{bmatrix} Y_{ac} \end{bmatrix} = \begin{bmatrix} 1 & 0 & 0 & 0 \\ 0 & 1 & 0 & 0 \\ 0 & 0 & 1 & 0 \\ 0 & 0 & 0 & 1 \end{bmatrix} \begin{bmatrix} I_{sq} \\ I_{sd} \\ V_{gq} \\ V_{gd} \end{bmatrix} \tag{5.44}$$

5.3.5 AC grid model with filters

With respect to the previous model, it is possible to incorporate filter behaviour. Instead of designing the capacitor for compensation of nominal reactive power, the following criteria are considered:

- One singled-tuned filter for the most prevalent harmonic (5^{th} for a 6-pulse or 11^{th} in a 12-pulse), which also compensates for 25% of the nominal reactive power;
- One singled-tuned filter for the second most prevalent harmonic(7^{th} for a 6-pulse or 13^{th} in a 12-pulse), which also compensates for 25% of the nominal reactive power;
- One three-phase capacitor bank, to compensate for half the nominal reactive power.

Note that the same method described here can be reproduced to add any number of filters, such as high-pass filters. With this in mind, the modelled grid is shown in the following figure:

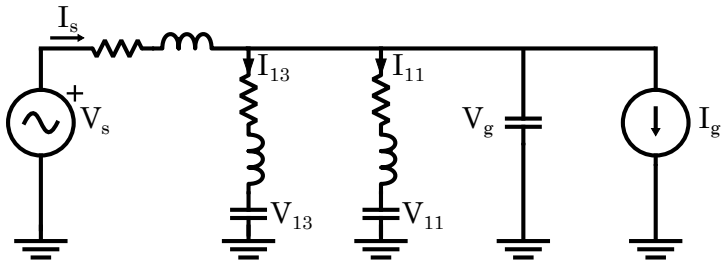

Figure 5.3: Modelled AC system including filter dynamics

The state variables are chosen to be the inductor current and capacitor voltages as usual. Note that the 11 and 13 subscripts are referred to a 12-pulse configuration, and should be replaced by the 5 and 7 subscripts in a 6-pulse system. The following equations describe the system behaviour:

$$V_{s,abc} - V_{g,abc} = r_s i_{s,abc} + l_s \frac{d}{dt} i_{s,abc} \tag{5.45}$$

$$V_{g,abc} - V_{13,abc} = r_{13} i_{13,abc} + l_{13} \frac{d}{dt} i_{13,abc} \tag{5.46}$$

$$V_{g,abc} - V_{11,abc} = r_{11} i_{11,abc} + l_{11} \frac{d}{dt} i_{11,abc} \tag{5.47}$$

$$C_{ac} \frac{d}{dt} V_{g,abc} = i_{s,abc} - i_{13,abc} - i_{11,abc} - i_{g,abc} \tag{5.48}$$

$$C_{13} \frac{d}{dt} V_{13,abc} = i_{13,abc} \tag{5.49}$$

$$C_{11} \frac{d}{dt} V_{11,abc} = i_{11,abc} \tag{5.50}$$

Once expressed in the q-d reference frame, these equations yield the following result:

$$
\begin{bmatrix} \dot{I}_{sq} \\ \dot{I}_{sd} \\ \dot{I}_{13q} \\ \dot{I}_{13d} \\ \dot{I}_{11q} \\ \dot{I}_{11d} \\ \dot{V}_{gq} \\ \dot{V}_{gd} \\ \dot{V}_{13q} \\ \dot{V}_{13d} \\ \dot{V}_{11q} \\ \dot{V}_{11d} \end{bmatrix} =
\begin{bmatrix}
\frac{-r_s}{l_s} & -\omega & 0 & 0 & 0 & 0 & 0 & 0 & 0 & 0 & 0 & 0 \\
\omega & \frac{-r_s}{l_s} & 0 & 0 & 0 & 0 & 0 & 0 & 0 & 0 & 0 & 0 \\
0 & 0 & \frac{-r_{13}}{l_{13}} & \omega & 0 & 0 & 0 & 0 & 0 & 0 & 0 & 0 \\
0 & 0 & -\omega & \frac{-r_{13}}{l_{13}} & 0 & 0 & 0 & 0 & 0 & 0 & 0 & 0 \\
0 & 0 & 0 & 0 & \frac{-r_{11}}{l_{11}} & \omega & 0 & 0 & 0 & 0 & 0 & 0 \\
0 & 0 & 0 & 0 & -\omega & \frac{-r_{11}}{l_{11}} & 0 & 0 & 0 & 0 & 0 & 0 \\
\frac{-1}{l_s} & 0 & \frac{1}{l_{13}} & 0 & \frac{1}{l_{11}} & 0 & 0 & \omega & 0 & 0 & 0 & 0 \\
0 & \frac{-1}{l_s} & 0 & \frac{1}{l_{13}} & 0 & \frac{1}{l_{11}} & -\omega & 0 & 0 & 0 & 0 & 0 \\
0 & 0 & 0 & \frac{-1}{l_{13}} & 0 & 0 & 0 & 0 & 0 & \omega & 0 & 0 \\
0 & 0 & 0 & 0 & \frac{-1}{l_{13}} & 0 & 0 & 0 & -\omega & 0 & 0 & 0 \\
0 & 0 & 0 & 0 & 0 & \frac{-1}{l_{11}} & 0 & 0 & 0 & 0 & \omega & 0 \\
0 & 0 & 0 & 0 & 0 & 0 & \frac{-1}{l_{11}} & 0 & 0 & 0 & 0 & -\omega \\
\end{bmatrix}
\begin{bmatrix} I_{sq} \\ I_{sd} \\ I_{13q} \\ I_{13d} \\ I_{11q} \\ I_{11d} \\ V_{gq} \\ V_{gd} \\ V_{13q} \\ V_{13d} \\ V_{11q} \\ V_{11d} \end{bmatrix}
+
\begin{bmatrix}
0 & 0 & 0 & 0 \\
0 & 0 & 0 & 0 \\
0 & 0 & 0 & 0 \\
0 & 0 & 0 & 0 \\
0 & 0 & 0 & 0 \\
0 & 0 & \frac{-1}{C_{ac}} & 0 \\
0 & \frac{-1}{C_{ac}} & 0 & 0 \\
0 & 0 & 0 & 0 \\
0 & 0 & 0 & 0 \\
0 & 0 & 0 & 0 \\
0 & 0 & 0 & 0 \\
0 & 0 & 0 & 0
\end{bmatrix}
\begin{bmatrix} I_{gq} \\ I_{gd} \\ V_{sq} \\ V_{sd} \end{bmatrix}
\tag{5.51}
$$

5.4 Small-signal complete model

The previous sections have shown how to build the basic blocks for representing a LCC-HVDC system in the state-space representation. The following figure will help understand how every one of the systems falls into place, as well as the role of the algebraic gains previously defined.

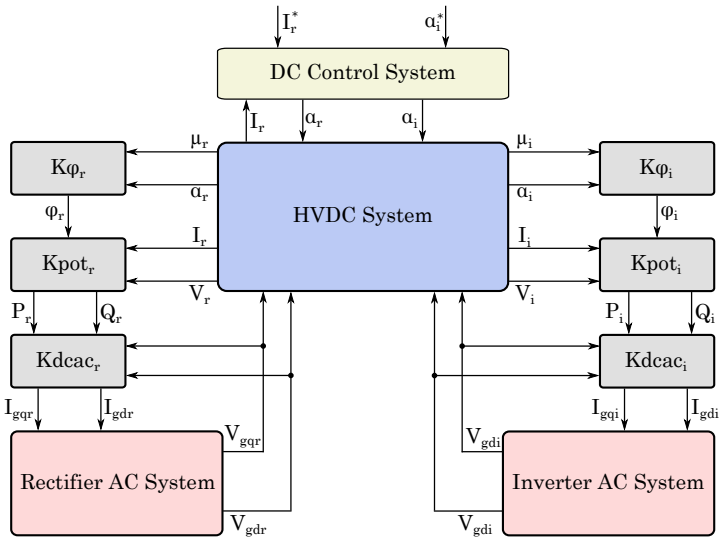

Figure 5.4: Complete system model

Figure 5.4 summarizes the whole small-signal model. Note that despite not having the Δ symbol, this model is indeed built with incremental variables. Only input and output variables that are inter-fed between models are represented. The grey-shaded blocks correspond to algebraic equations, i.e. without implying derivatives. They serve uniquely to link the different dynamic systems. On the other hand, colour-shaded blocks do represent dynamic systems:

- The blue-shaded HVDC system is the centrepiece of the model, and represents (5.10) and (5.13);
- The yellow-shaded DC control block encompasses eq. (5.27) and (5.28);
- $K\varphi_r$ and $K\varphi_i$ represent eq. (5.31) and (5.32);
- $KPot_r$ and $KPot_i$ represent eq. (5.35) and (5.36);
- $Kdcac_r$ and $Kdcac_i$ represent eq. (5.39), either taking the rectifier or inverter variables;
- Finally, the red-shaded HVAC systems represent the dynamic behaviour around the AC converter terminals, which can be represented either by (5.43) (no filters) or by (5.51) which includes filter dynamics. It is recommended that both sides (rectifier and inverter) use the same equation type, using the appropriate parameters.

It should be also said that some authors prefer complete state representation, that is including all systems and gains in a single state-space representation. In this case, this would correspond

to a 27^{th} order state matrix, which would be difficult to read but especially difficult to modify. The advantage of employing a disaggregate system representation is the ease of modification. For example, the control strategy can be modified without having to change the terms of a large and complex 27^{th} order matrix. It is much easier to modify parts of the model with this disaggregate approach. Additionally, mistakes are much clear to track and the role of each part is easier to understand.

Chapter 6

Case study

6.1 Introduction

This sections aims to validate the small-signal model built in the previous sections. For this reason, the small-signal LCC model will be tested against a non-linear model. The dynamics and steady-state values of the small-signal model should reproduce quite accurately the behaviour of the non-linear model. Moreover, a mathematical analysis on the space-state system will be performed, based on participation factors. The results of this latter mathematical analysis should also be verified in the non-linear model.

6.2 Case Study Description

The studied case corresponds to a LCC transmission system situated between Balearic Islands and the Spanish mainland. However, as the official project data is not openly available, the system parameters will be evaluated thanks to CIGRE available parameters [13]. A single-pole system will be simulated, comparing results of the small-signal model with the non-linear one. The value of the parameters is shown in Table 6.1. On the other hand, fig. 6.1 shows a schematic of the simulated system as well as indicates the system parameters.

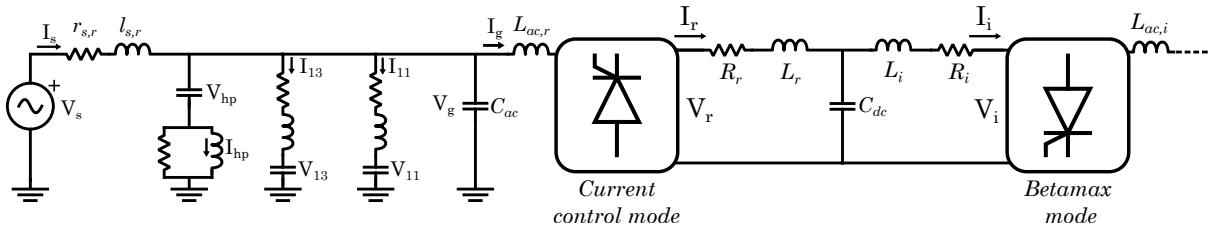

Figure 6.1: Schematic of the case study modelled system

Table 6.1: Case study parameter values

Parameter	Value	Units
L_r	0.748	H
R_r	2.5723	Ω
L_i	0.748	H
R_i	2.5723	Ω
C_{dc}	26	μF
$L_{ac,r}$	0.0103	H
$L_{ac,i}$	0.0103	H
$r_{s,r}$	0.098	Ω
$l_{s,r}$	0.0032	H
$r_{s,i}$	0.098	Ω
$l_{s,i}$	0.0032	H

6.2.1 System operating point

As a first step, the non-linear model is run, which allows to obtain all the necessary data for the linearisation point needed for the small-signal model. Note that for this standard operational point, it is assumed that the controls of the rectifier are in constant current mode, and the inverter is in Betamax mode. The following table shows the values of the operating point:

Table 6.2: Values corresponding to the operating point

Parameter	Value	Units
α_{r0}	27.9	°
α_{i0}	150	°
V_{c0}	250.25	kV
I_{r0}	800	A
I_{i0}	800	A
P_{r0}	201.85	MW
Q_{r0}	103.8	Mvar
P_{i0}	200.01	MW
Q_{i0}	115.5	Mvar
V_{r0}	252.3	kV
V_{i0}	248.25	kV

Those values correspond to the operating point of the non-linear model, and therefore define the linearisation point of the small-signal model. They are also used for control tuning in the next subsection.

6.2.2 Control tuning

The first control objective is to design a control system to achieve normal operation of an LCC-HVDC link, i.e. fixing the extinction angle of the inverter and designing a control system enabling a controlled constant current at the rectifier. Therefore, the first step is to design a controller to achieve constant current. The input of the controller would be the current reference and its output the firing angle α. In order to design the controller, one must know the plant transfer function, which can be obtained from the state-space model given by (5.7), and an output equation formed by an identity matrix.

$$W(s) = C(sI - A)^{-1} B + D \tag{6.1}$$

This yields a 4x4 transfer function matrix. In order to tune the controllers for the dc current control, the transfer function of position (1,3) is considered, corresponding to $\Delta\alpha_r$ as the input and I_r as the output. A PI controller with α_r as output variable is then tuned, accounting for a settling time of 100 ms and a damping of 0.707. Note that the controller parameters are tuned for a determined linearisation point. It implies that for any large parameter modification (voltage level, nominal power), the controller performance can not be guaranteed. Other more refined control approaches could be possible (such as H_∞ techniques), however the focus of this project is constructing the model and not optimising the control strategy.

6.2.3 Effect of the reference filter on the DC system response

Sending a direct step reference ultimately triggers excitation of all potential modes, and is generally avoided for this reason. It is interesting to analise how does the filter effects the response of the DC system. For this reason, the DC current I_r response with respect to the reference I_r^* is studied, comparing a filtered reference with a direct unfiltered step reference, by means of a bode plot shown in fig. 6.2. Note how the system response at higher frequencies is substantially improved without affecting the system tracking capability at 0 Hz. On the other hand, adding the filter implies some delay on the system. It is however very interesting to isolate the DC system from the higher frequencies, as AC harmonics that can propagate to the DC side by means of the DC voltage will not affect the tracking capability of the control system.

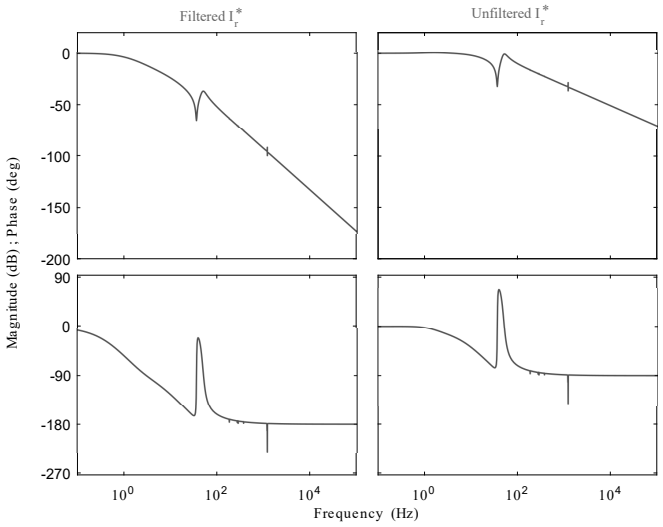

Figure 6.2: Bode plot of the DC system response with and without filtered reference

6.2.4 Analysis description

Both models are subjected to a current reference increase of 100 A from the operational point. The current reference evolution is limited through a first-order filter with a time constant of 200 ms, in order to avoid exciting resonances on the AC system. The dynamics and steady-state values of both system should be correspondent. However, some differences are to be expected, as the small-signal model corresponds to a linear approximation of the system behaviour. It should also be added that in order to be able to measure the mean values of signals, all measurements form the non-linear model are filtered with a first-order filter. The following figure shows the effect of the filter and proves its necessity.

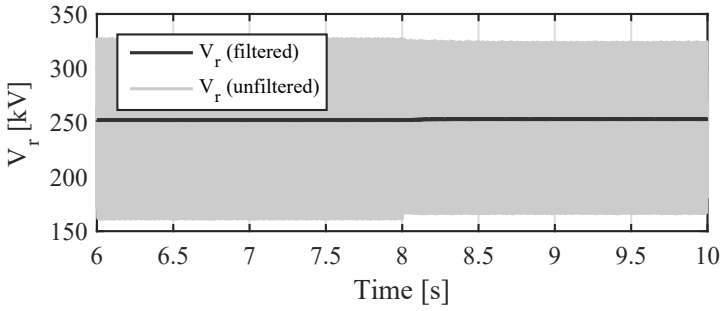

Figure 6.3: Comparison between filtered and unfiltered DC rectifier terminal voltage

Note from the figure that it is extremely difficult to estimate the mean value of the signal, and therefore changes in values experienced due to the reference change would be difficult to track, thereby justifying the need of filters. Moreover, in order to guarantee consistency of the results, the same filters are applied to the small-signal model results, hence allowing to compare the signals of both models. Necessarily, this implies loss of information at some degree, as some frequencies are filtered out.

6.3 Case results comparison

This section draws the comparison between the non-linear model and the small signal model. It is expected that both models yield similar steady-state results, although some differences are to be expected due to the linearisation process. In fact, as an increase of 100A corresponds to a deviation of 12.5% from the operational point, which is certainly enough to produce some small discrepancies. Figures 6.4 through 6.14 show the comparison between the different models, for various signals.

For the majority of figures, the small-signal model displays a high accuracy. Higher deviations are seen regarding reactive power and the AC current d-component. For instance, calculation of the linearised reactive power comes from non-linear composed trigonometrical functions. Hence, such deviations are deemed to be expected, as linearisation errors propagate through consecutive steps, yielding a lower accuracy. Furthermore, the AC current d-component is strongly related to the reactive power, thereby propagating linearisation errors.

Still, the small-signal model can be considered validated, and therefore approved to be used in future studies.

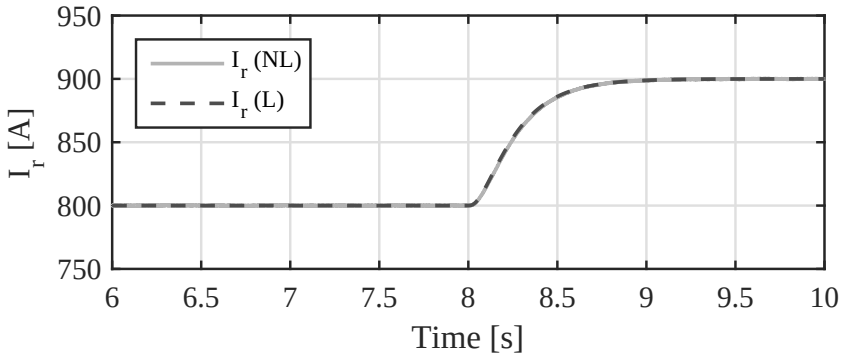

Figure 6.4: Comparison of rectifier DC current for both models

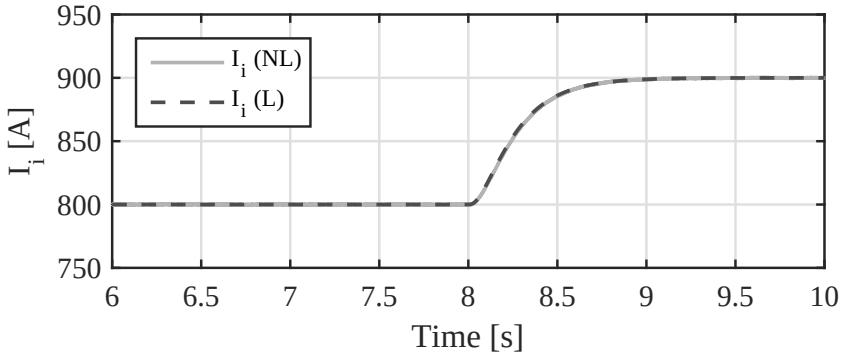

Figure 6.5: Comparison of inverter DC current for both models

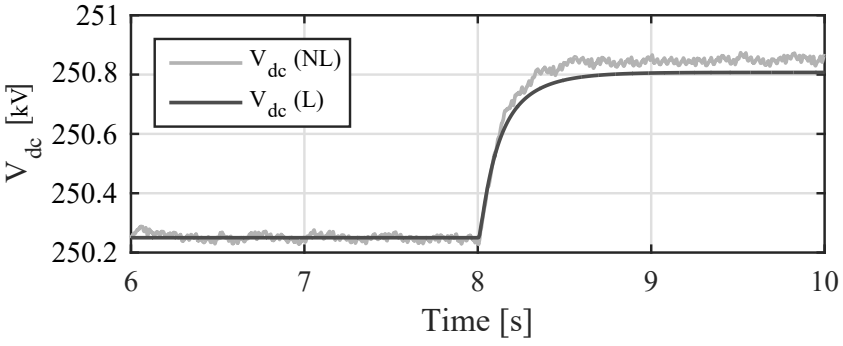

Figure 6.6: Comparison of midpoint DC voltage level for both models

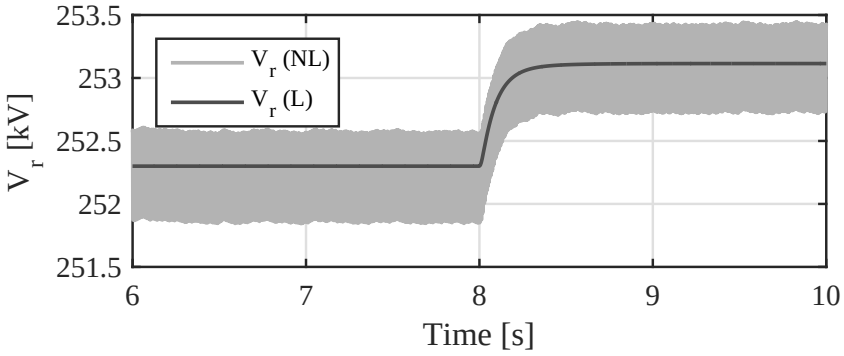

Figure 6.7: Comparison of rectifier DC terminal voltage level for both models

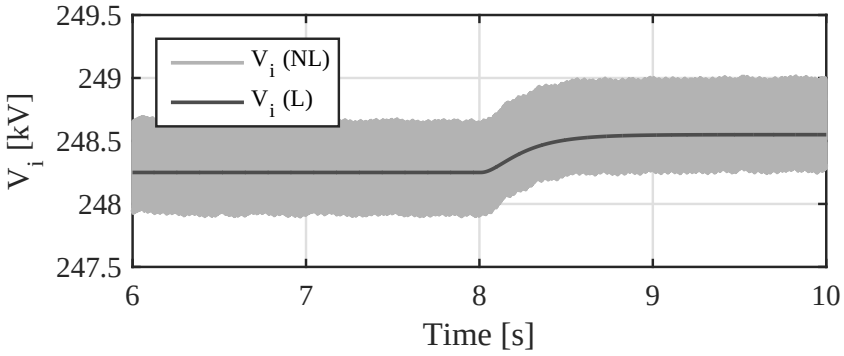

Figure 6.8: Comparison of inverter DC terminal voltage level for both models

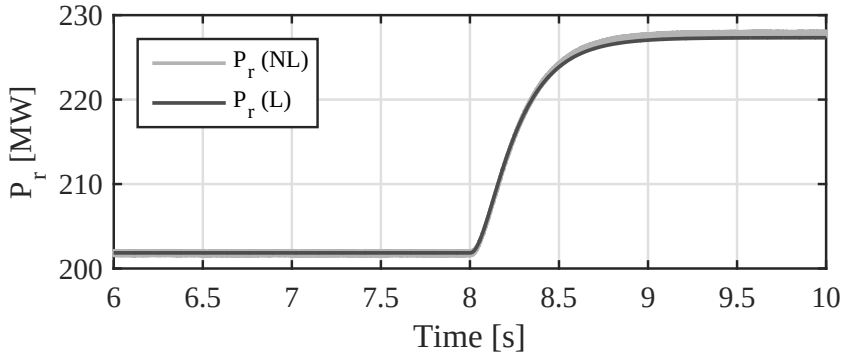

Figure 6.9: Comparison of rectifier active power for both models

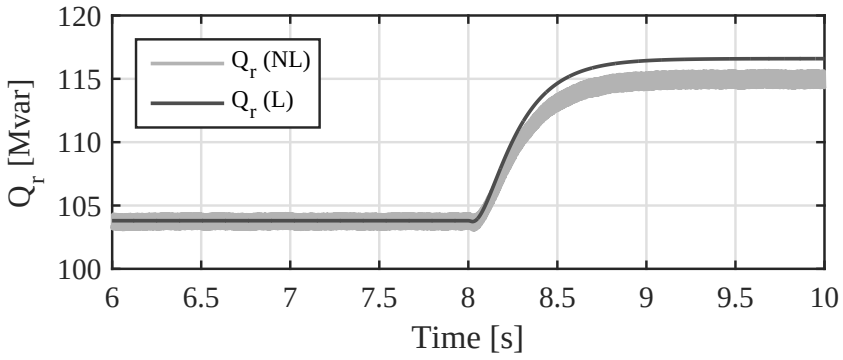

Figure 6.10: Comparison of rectifier reactive power for both models

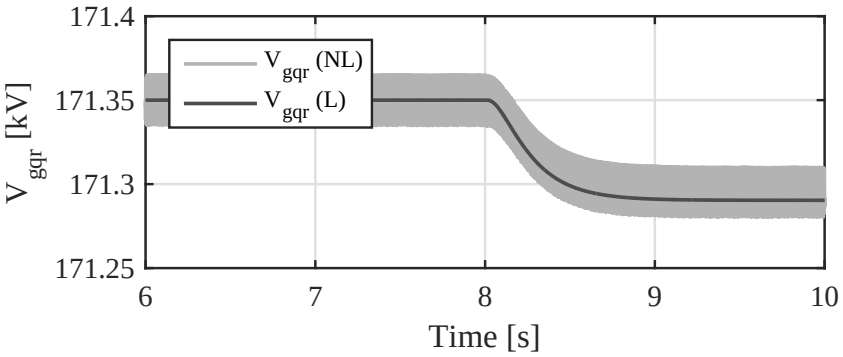

Figure 6.11: Comparison of q component of the rectifier AC terminal voltage for both models

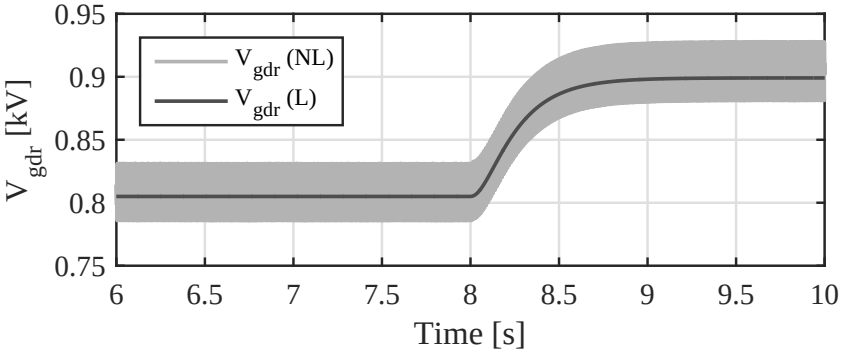

Figure 6.12: Comparison of d component of the rectifier AC terminal voltage for both models

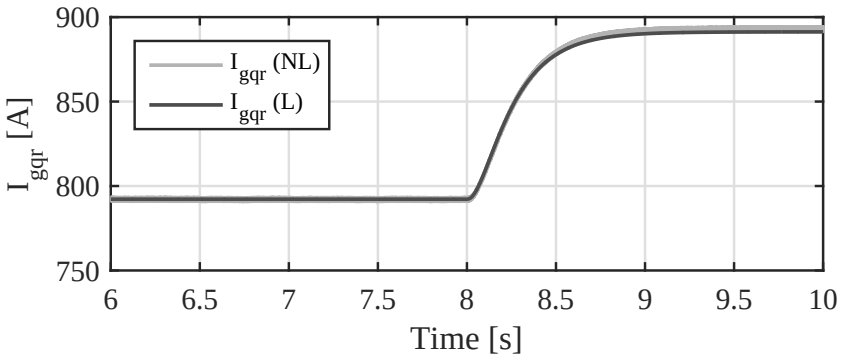

Figure 6.13: Comparison of q component of the rectifier AC current for both models

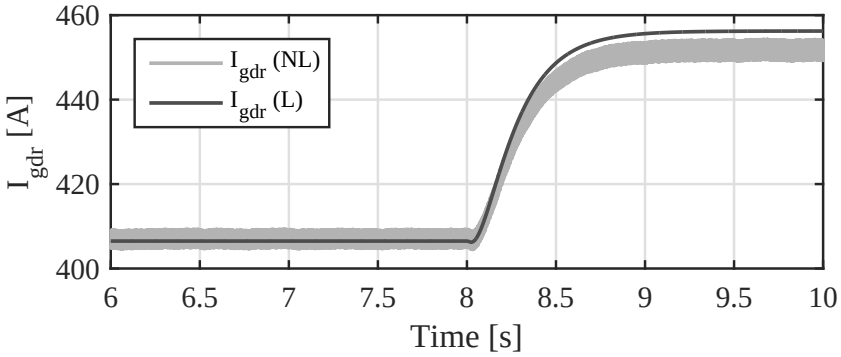

Figure 6.14: Comparison of d component of the rectifier AC current for both models

6.4 Non-linear model system response

The previous section has validated the small-signal model with respect to the non-linear model. However, as the outputs of the non-linear model have been filtered in order to compare the results, the real waveforms of the variables has not been shown. Consequently, fig. 6.15 through 6.38 show the evolution of the system variables without filters. Note that by comparing fig. 6.37 and 6.38, the effect of the AC filters can be observed.

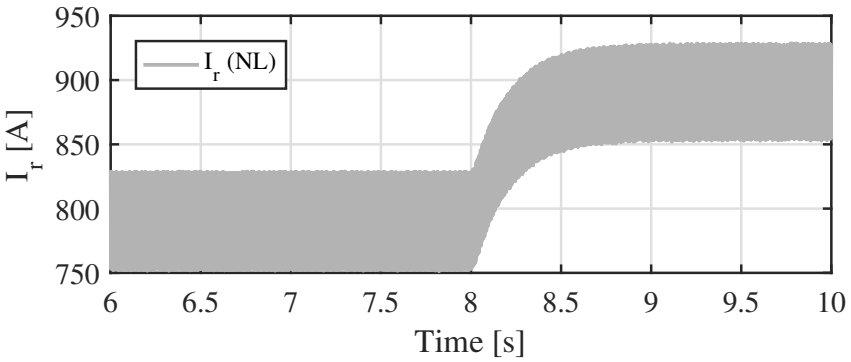

Figure 6.15: Current at the rectifier DC terminal

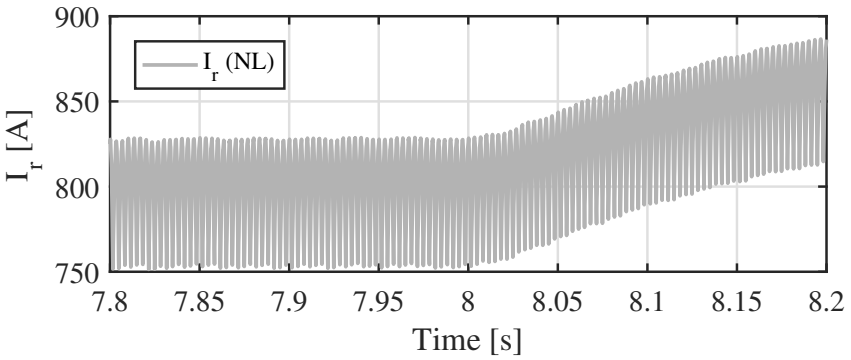

Figure 6.16: Zoomed current at the rectifier DC terminal

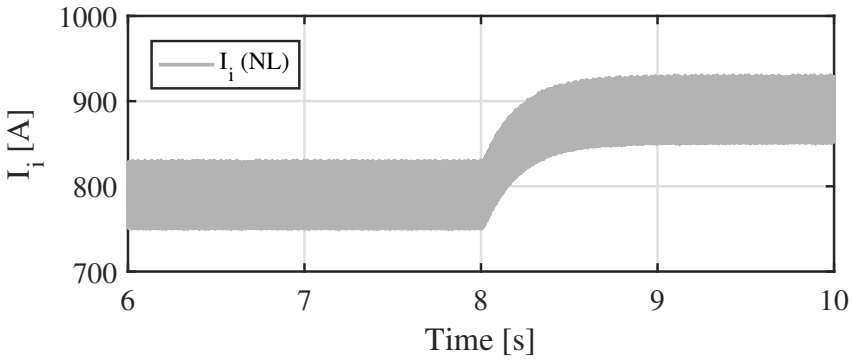

Figure 6.17: Current at the inverter DC terminals

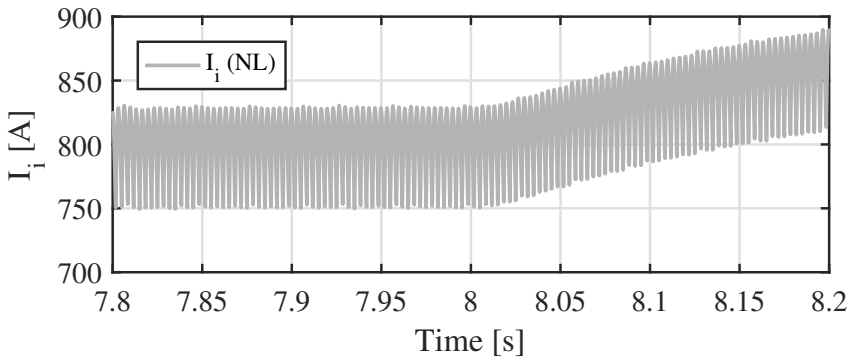

Figure 6.18: Zoomed current at the inverter DC terminal

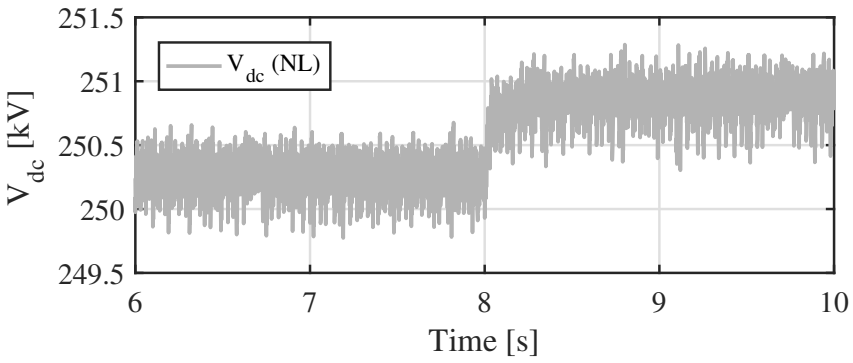

Figure 6.19: Voltage level at the DC midpoint capacitor

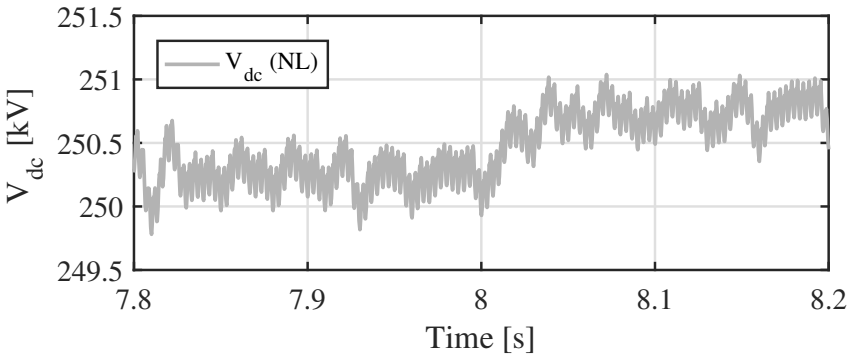

Figure 6.20: Zoomed voltage level at the DC midpoint capacitor

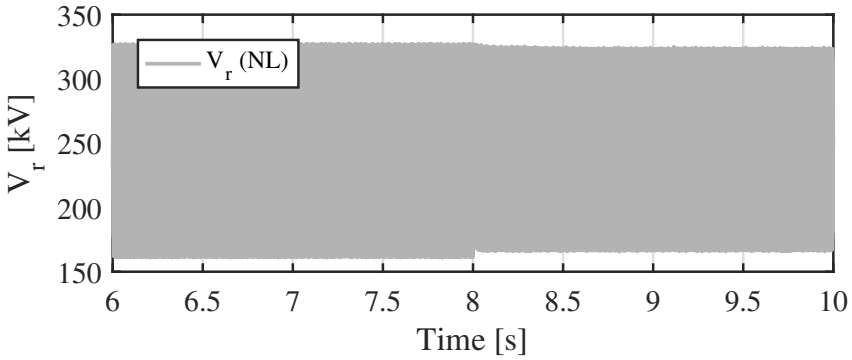

Figure 6.21: Voltage level at the rectifier DC terminal

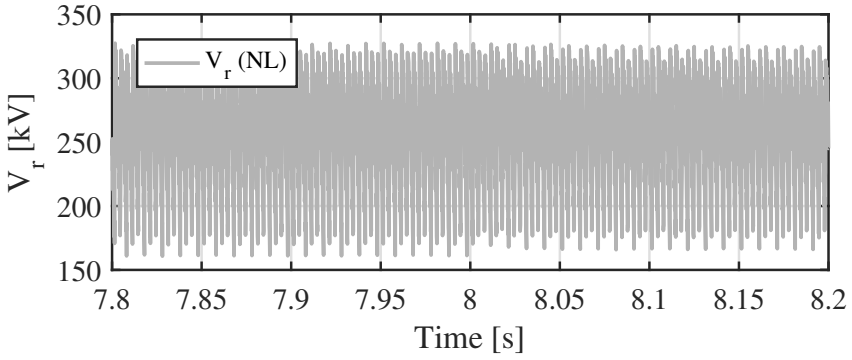

Figure 6.22: Zoomed voltage level at the rectifier DC terminal

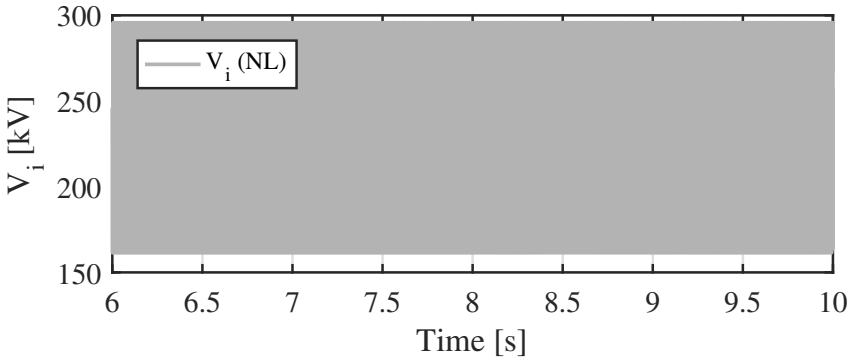

Figure 6.23: Voltage level at the inverter DC terminal

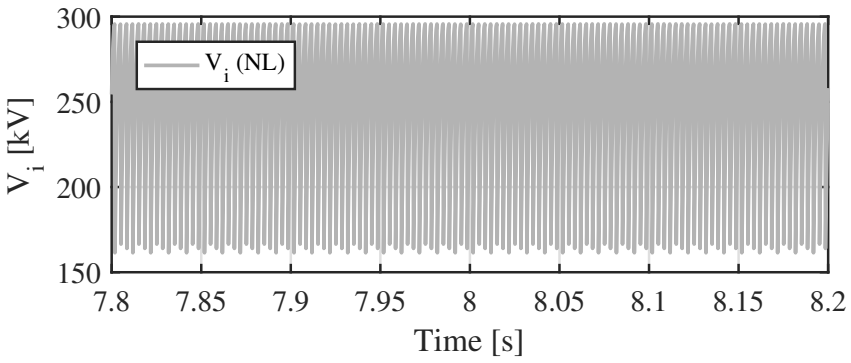

Figure 6.24: Zoomed voltage level at the inverter DC terminal

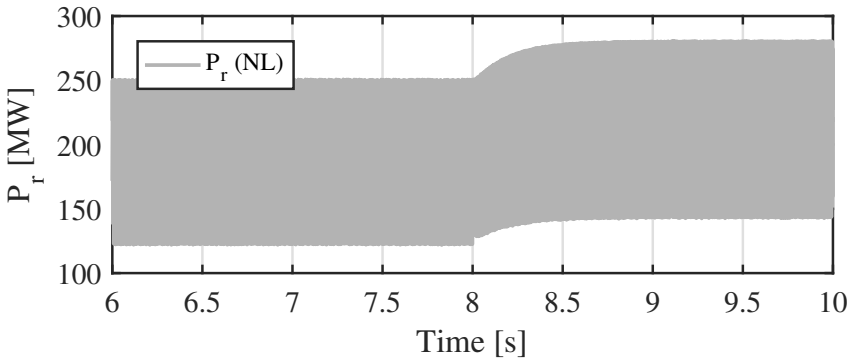

Figure 6.25: Active power at the rectifier AC terminal

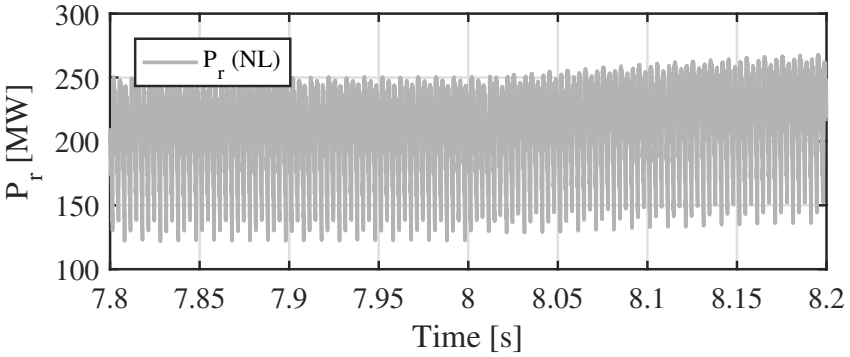

Figure 6.26: Zoomed active power at the rectifier AC terminal

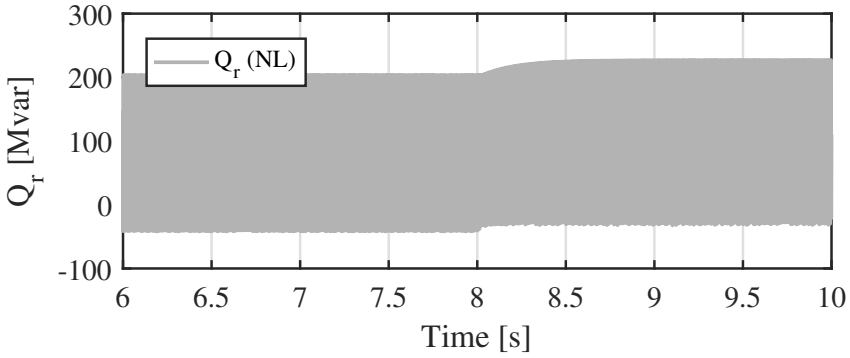

Figure 6.27: Reactive power at the rectifier AC terminal

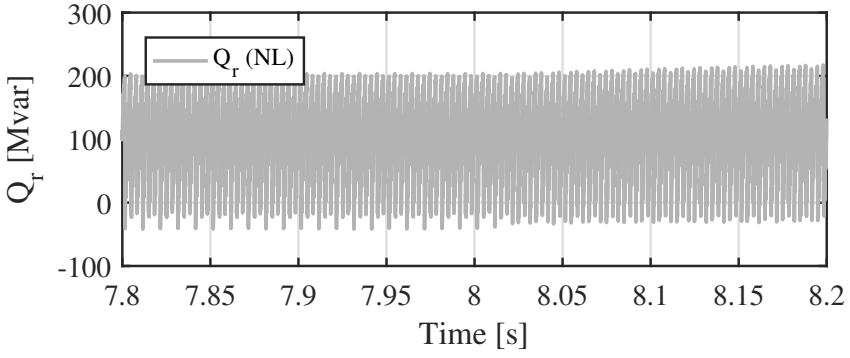

Figure 6.28: Zoomed reactive power at the rectifier AC terminal

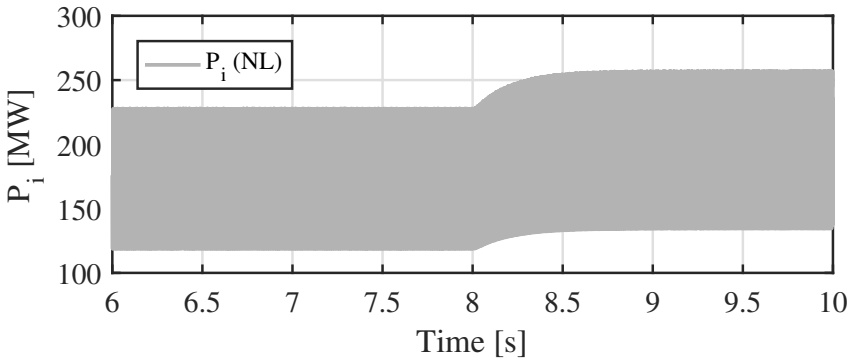

Figure 6.29: Active power at the inverter AC terminal

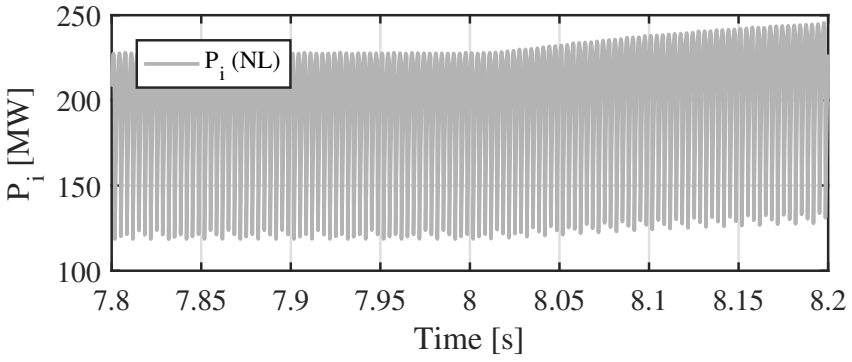

Figure 6.30: Zoomed active power at the inverter AC terminal

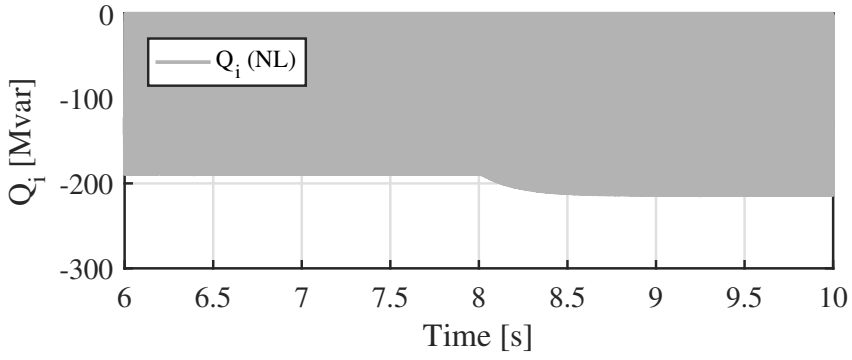

Figure 6.31: Reactive power at the inverter AC terminal

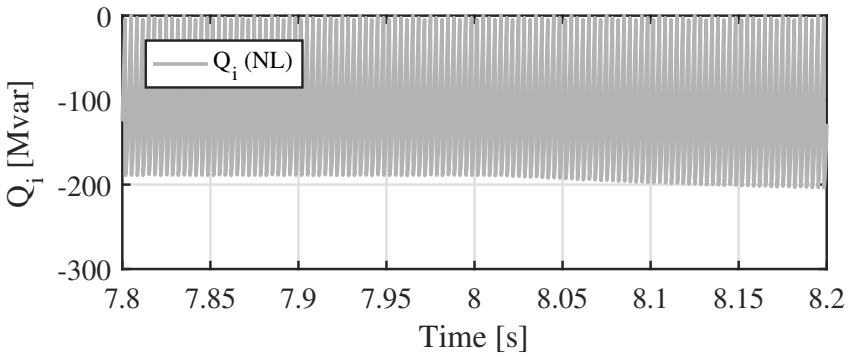

Figure 6.32: Zoomed reactive power at the inverter AC terminal

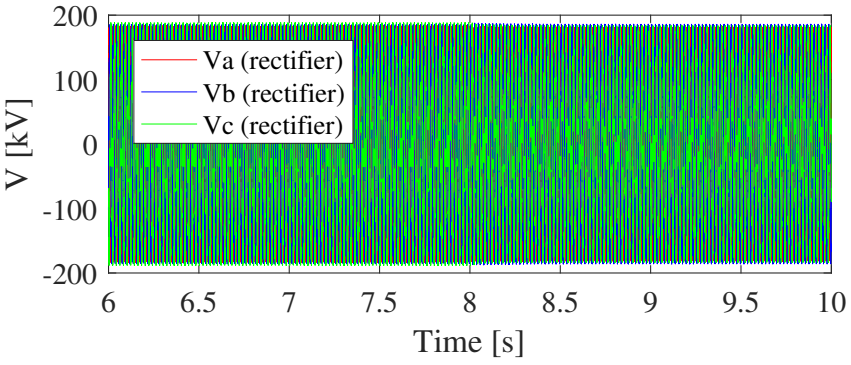

Figure 6.33: Voltage waveforms at the rectifier AC terminal

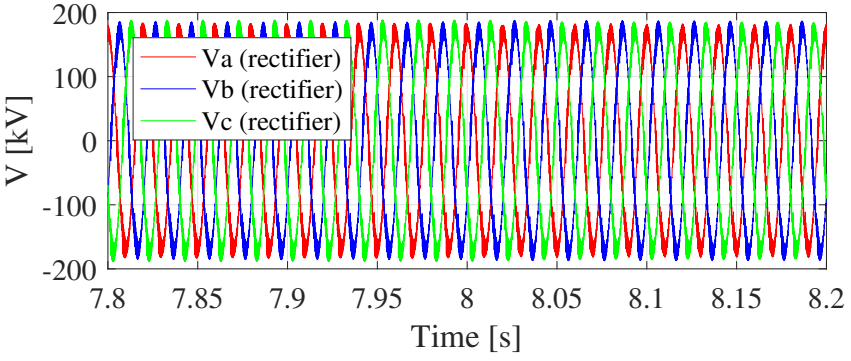

Figure 6.34: Zoomed voltage waveforms at the rectifier AC terminal

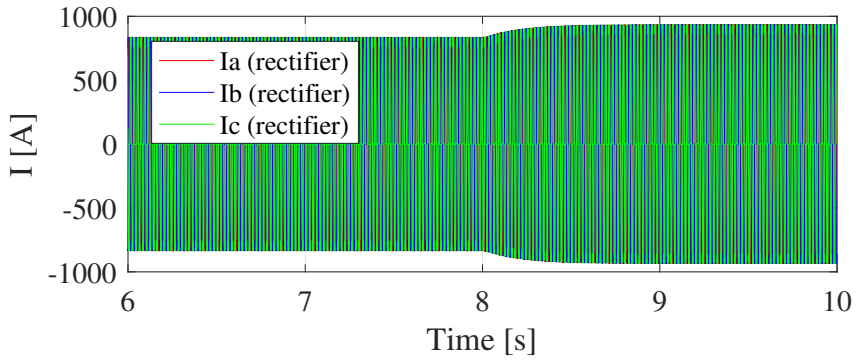

Figure 6.35: Current waveforms at the rectifier AC terminal

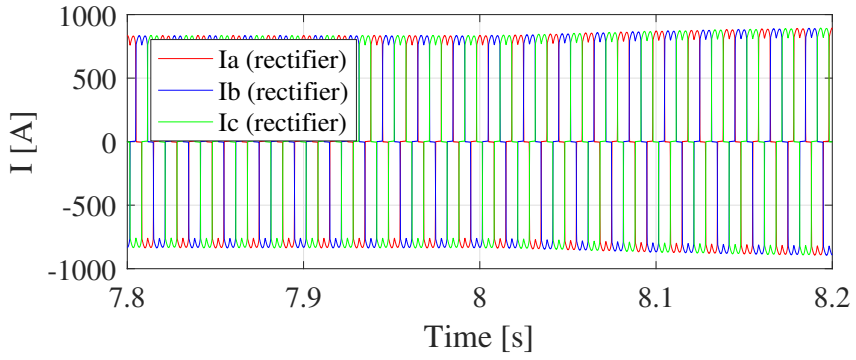

Figure 6.36: Zoomed current waveforms at the rectifier AC terminal

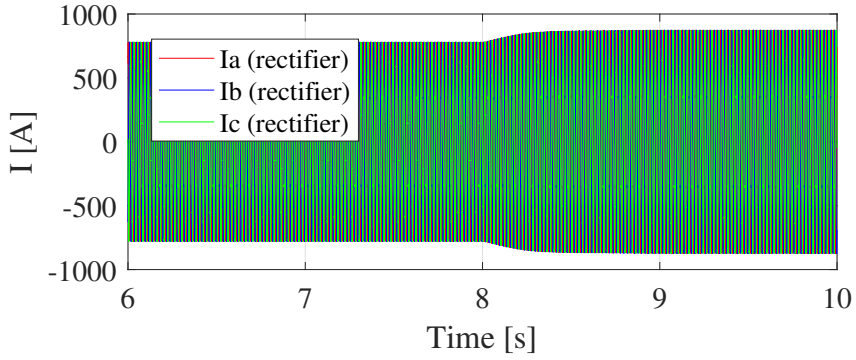

Figure 6.37: Current waveforms at the rectifier AC grid side

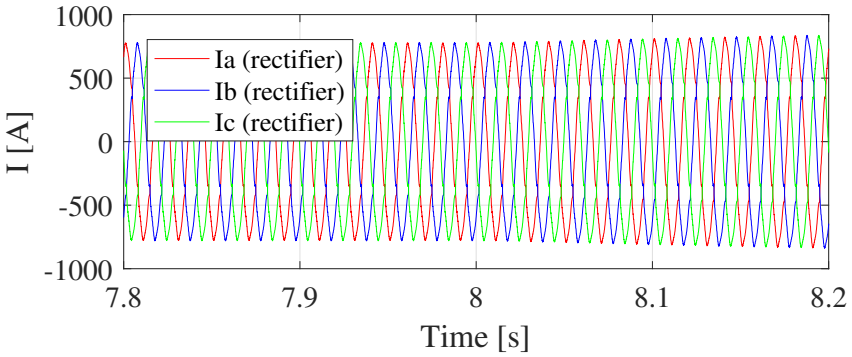

Figure 6.38: Zoomed current waveforms at the rectifier AC grid side

6.5 Small-signal model analysis

Unfortunately, the use of filters has hindered the possibility of visually comparing the dynamics of both models. However, a mathematical analysis of the small-signal model allows much clear results on the system dynamics. Furthermore, it decouples the natural system dynamics from the commutation-related dynamics, which may help for a better identification of potentially hazardous dynamics.

For this reason, the first step is to analyse the poles of the complete small-signal model, shown in Table 6.3

Table 6.3: Natural frequency and damping of the small-signal model poles

Natural frequency [Hz]	Damping
0.8	1
1.54	1
1.9	1
2	1
14.22	1
49.39	0.140
49.39	0.140
50	0.286
50	0.286
50	0.0025
50	0.0025
198.6	0.0001
198.6	0.0001
296.3	0.0020
296.3	0.0020
298.6	0.0001
298.6	0.0001
396.3	0.0015
396.3	0.0015
3374.1	0.0012
3374.1	0.0012
3377.9	0.0002
3377.9	0.0002

The pole analysis reveals two pairs of particularly low-damped high-frequency poles, indicating a high-frequency mode at around 3376 Hz. However, the damping remains positive, and on the other hand this resonance would only be triggered in very particular situations. However, sudden and rapid changes in the system inputs could potentially reveal a problematic resonance at this frequency. The participation factors analysis found in Table 6.4 helps tracking the source of this mode. Note that there are no missing modes: for sake of readability, twin modes have been removed from the table.

Table 6.4: Scaled modal participation factor for the standard case

	'Mode1'	'Mode3'	'Mode5'	'Mode7'	'Mode9'	'Mode11'	'Mode15'	'Mode17'
'f (Hz)'	3377.92	3374.09	396.31	296.32	298.62	198.63	47.90	48.90
'damp'	0.00023	0.0012	0.0019	0.00014	0.0001	0.00014	0.29	0.14
I_{sq}	0.80	0.78	0.02	0.02	0.01	0.01	0	0
I_{sd}	1.00	0.62	0.02	0.02	0.01	0.01	0	0
I_{7q}	0.02	0.02	0.98	0.98	0	0	0	0
I_{7d}	0.02	0.01	0.98	0.98	0	0	0	0
I_{5q}	0.01	0.01	0	0	0.99	0.99	0	0
I_{5d}	0.01	0.01	0	0	0.99	0.99	0	0
V_{gq}	0.67	1.00	0	0	0	0	0	0
V_{gd}	0.84	0.80	0	0	0	0	0	0
V_{7q}	0	0	1.00	1.00	0	0	0	0
V_{7d}	0	0	1.00	1.00	0	0	0	0
V_{5q}	0	0	0	0	1.00	1.00	0	0
V_{5d}	0	0	0	0	1.00	1.00	0	0
I_{hpq}	0	0	0	0	0	0	0	0
I_{hpd}	0	0	0	0	0	0	0	0
V_{hpq}	0	0	0	0	0	0	1.00	0
V_{hpd}	0	0	0	0	0	0	1.00	0
$intI_r^*$	0	0	0	0	0	0	0	0
$intI_r$	0	0	0	0	0	0	0	0.01
I_r	0	0	0	0	0	0	0	0.47
I_i	0	0	0	0	0	0	0	0.54
V_{dc}	0	0	0	0	0	0	0	1.00

As it can be seen, the undamped high-frequency modes are linked with all AC variables, particularly with the source current and more importantly to the AC terminal converter voltage. In fact, during the AC harmonic filter tuning process, some parameters had to be determined in an iterative process, due to the presence of an unstable resonance in the kHz range. By increasing the damping of the high-frequency filter and slightly decreasing the capacitance of the capacitor bank, the resonant frequency was increased and its damping augmented. Therefore, this low-damped mode actually corresponds to the result of this iterative process.
Furthermore, it is interesting to see the relative participation of each variable, which can be observed in fig. 6.39.

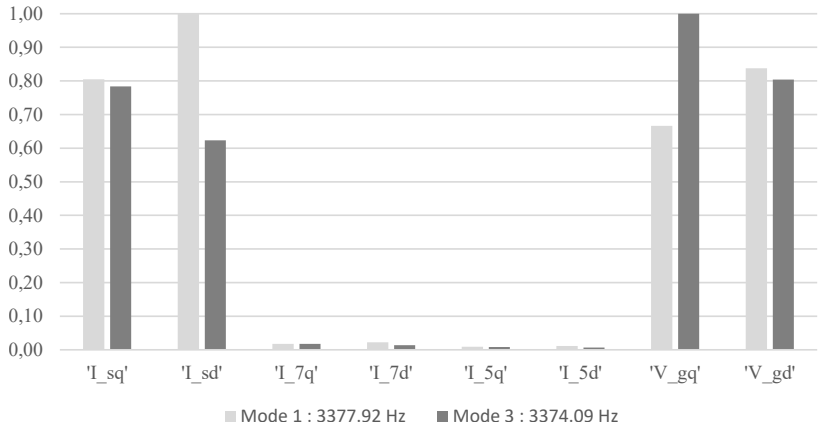

Figure 6.39: Relative participation factors of the AC variables on the high-frequency modes

The 17^{th} mode is also an interesting one, as it is uniquely participated by the DC variables. In fact, it corresponds with a resonant frequency between the DC-side capacitor and inductors. The relatively low resonant frequency can be explained by the large value of the DC inductances.

6.5.1 Influence of the grid strength on the system poles and participation factors

It is interesing to see the behaviour of the poles as the SCR diminishes (cf. Section 4.4.1). For this reason, the L_{ac} parameter is increased up to equivalent values of SCR of 5, 3 and 2. Theoretically, low SCRs (e.g. SCR=2) should turn the system unstable with the implemented typical control loops.Tables 6.5, 6.6 and 6.7 show the poles and participation factors for each respective case.

Table 6.5: Scaled modal participation factor for SCR=5

	'Mode1'	'Mode3'	'Mode5'	'Mode7'	'Mode9'	'Mode11'	'Mode15'	Mode17'
'f (Hz)'	842.73	810.53	344.74	246.04	230.42	134.29	47.90	48.71
'damp'	0.0003	0.0022	0.0013	0.0017	0.0064	0.0089	0.2865	0.1428
V_{dc}	0.37	0.32	0.12	0.11	0.90	0.82	0	0
I_{sq}	0.43	0.26	0.12	0.12	0.88	0.77	0	0.01
I_{sd}	0.56	0.42	0.70	0.70	0.12	0.11	0	0
I_{7q}	0.65	0.34	0.71	0.71	0.10	0.11	0	0
I_{7d}	0.22	0.18	0.76	0.69	0.48	0.54	0	0
I_{5q}	0.26	0.15	0.75	0.65	0.53	0.54	0	0
I_{5d}	0.82	1.00	0.04	0.04	0.12	0.11	0	0
V_{gq}	1.00	0.86	0.04	0.04	0.11	0.11	0	0
V_{gd}	0.12	0.06	0.99	0.96	0.44	0.41	0	0
V_{7q}	0.13	0.05	1.00	1.00	0.41	0.40	0	0
V_{7d}	0.02	0.01	0.54	0.50	0.94	1.00	0	0
V_{5q}	0.03	0.01	0.54	0.46	1.00	0.98	0	0
V_{5d}	0.01	0.01	0	0	0.03	0.03	0	0
I_{hpq}	0.01	0.01	0	0	0.03	0.03	0	0
I_{hpd}	0	0	0	0	0	0	1.00	0
V_{hpq}	0	0	0	0	0	0	1.00	0
V_{hpd}	0	0	0	0	0	0	0	0
$intI_r^*$	0	0	0	0	0	0	0	0.01
$intI_r$	0	0	0	0	0	0	0	0.46
I_r	0	0	0	0	0	0	0	0.54
I_i	0	0	0	0	0	0	0	1.00

Table 6.6: Scaled modal participation factor for SCR=3

	'Mode1'	'Mode3'	'Mode5'	'Mode7'	'Mode9'	'Mode11'	Mode15'	Mode17'
'f (Hz)'	790.07	752.79	340.09	241.43	202.59	108.55	47.90	48.52
'damp'	0.0002	0.0019	0.0009	0.0013	0.0085	0.0116	0.2865	0.1449
V_{dc}	0.25	0.22	0.08	0.08	1.00	1.00	0	0
I_{sq}	0.29	0.19	0.08	0.09	1.00	0.89	0	0.01
I_{sd}	0.69	0.52	0.63	0.68	0.09	0.10	0	0
I_{7q}	0.79	0.44	0.64	0.69	0.09	0.10	0	0
I_{7d}	0.26	0.21	1.00	0.98	0.26	0.34	0	0
I_{5q}	0.30	0.18	1.00	0.95	0.29	0.34	0	0
I_{5d}	0.84	1.00	0.05	0.05	0.16	0.16	0	0
V_{gq}	1.00	0.88	0.05	0.05	0.16	0.16	0	0
V_{gd}	0.16	0.09	0.92	0.98	0.46	0.50	0	0
V_{7q}	0.18	0.07	0.93	1.00	0.46	0.48	0	0
V_{7d}	0.03	0.02	0.74	0.72	0.73	0.86	0	0
V_{5q}	0.04	0.02	0.74	0.69	0.78	0.84	0	0
V_{5d}	0.01	0.01	0.01	0.01	0.05	0.05	0	0
I_{hpq}	0.02	0.01	0.01	0.01	0.05	0.05	0	0
I_{hpd}	0	0	0	0	0	0	1.00	0
V_{hpq}	0	0	0	0	0	0	1.00	0
V_{hpd}	0	0	0	0	0	0	0	0
$intI_r^*$	0	0	0	0	0	0	0	0.01
$intI_r$	0	0	0	0	0	0.03	0	0.46
I_r	0	0	0	0	0	0	0	0.55
I_i	0	0	0	0	0	0	0	1.00

Table 6.7: Scaled modal participation factor for SCR=2

	'Mode1'	'Mode3'	'Mode5'	'Mode7'	'Mode9'	'Mode11'	'Mode15'	Mode17'
'f (Hz)'	750.14	708.17	336.65	237.95	166.95	75.94	47.90	47.74
'damp'	-7E+05	0.002	0.001	0.001	0.011	0.011	0.286	0.151
V_{dc}	0.14	0.13	0.04	0.04	0.98	1.00	0	0.01
I_{sq}	0.16	0.11	0.04	0.04	1.00	0.76	0	0.04
I_{sd}	0.83	0.63	0.47	0.52	0.05	0.06	0	0
I_{7q}	0.93	0.54	0.48	0.53	0.05	0.06	0	0
I_{7d}	0.30	0.25	1.00	1.00	0.11	0.16	0	0
I_{5q}	0.34	0.22	1.00	0.98	0.13	0.16	0	0
I_{5d}	0.85	1.00	0.04	0.04	0.18	0.19	0	0
V_{gq}	1.00	0.89	0.04	0.04	0.18	0.18	0	0
V_{gd}	0.22	0.13	0.70	0.77	0.44	0.49	0	0.01
V_{7q}	0.24	0.10	0.71	0.78	0.46	0.47	0	0.01
V_{7d}	0.04	0.03	0.76	0.76	0.54	0.66	0	0.01
V_{5q}	0.04	0.02	0.76	0.74	0.59	0.63	0	0.01
V_{5d}	0.02	0.01	0	0	0.11	0.11	0	0
I_{hpq}	0.02	0.01	0	0	0.11	0.08	0	0
I_{hpd}	0	0	0	0	0	0	1.00	0
V_{hpq}	0	0	0	0	0	0	1.00	0
V_{hpd}	0	0	0	0	0	0	0	0
$intI_r^*$	0	0	0	0	0	0	0	0.01
$intI_r$	0	0	0	0	0.01	0.13	0	0.42
I_r	0	0	0	0	0	0.01	0	0.56
I_i	0	0	0	0	0	0.05	0	1.00

Several interesting facts can be observed from the previous results:

- Effectively, for a SCR of 2, there is an unstable mode, related to the AC converter terminal voltage V_g. This is very consistent with the literature, as it coincides in the SCR value as well as in the unstable variable; which further proves the validity of this model. On the other hand, alternative control strategies should be envisaged for these cases with SCR lower than 3.
- The lower the SCR, the more the modes are connected. Note how the number of participation factors above zero increase in the case of low SCRs, particularly when compared to the standard case, where the grid is much stronger (cf. Table 6.4).
- The DC-linked mode (mode 17) remains largely unaffected by the value of the SCR. Despite the AC converter voltage having a strong effect in the DC-side voltage, the mode behaviour seems to be quite independent from the AC-side modes. The participation factors related to this mode remain mostly the same, excepting that with the lower SCR there is some participation of the AC current in the DC mode. On the other hand, the damping and frequency of the mode stays largely the same throughout the SCR sweep.

6.5.2 Response of the non-linear model against a low SCR condition

The previous section has studied the effect of a low SCR (i.e. a weak grid situation) by means of a mathematical analysis of the small-signal model. In this section, the same effect will be studied on the non-linear model. A low SCR scenario may happen because of a sudden change in the grid conditions at one of the two terminals, such as the tripping of one line at the inverter terminal. This is the condition that is studied here: the system will first reach steady-state operation point, then secondly one of the AC lines connected to the inverter terminals is disconnected. This causes a low SCR condition on the inverter terminals, which should cause undesirable conditions throughout the transmission system.

The simulations develops as follows:

- The model is started and progressively reaches the operation point
- Once the system is in its stable operational point, a sudden decrease in the SCR at the inverter grid is provoked (c.f. fig. D.4), up to a value of 1.5. This will be executed by opening the breakers of parallel lines, at t=3.2s
- It is expected that the increase in SCR at the inverter AC system will cause contingencies through the LCC-HVDC transmission system.

Figures 6.40 and 6.41 show the system response in front of the decrease of the SCR. Effectively, there has been a contingency, which is a commutation failure. The low SCR (i.e., large commutating inductance) has provoked that the commutation process from phase c to phase a extends beyond 180°, which implies that the commutation cannot be completed, as the current of the phase c has not reached the zero value. Therefore, the commutation process is interrupted, triggering various conditions throughout the LCC-HVDC system. Note that, for the sake of clarity, the *abc* waveforms have been plotted using one colour for each phase, despite the other figures being black and white.

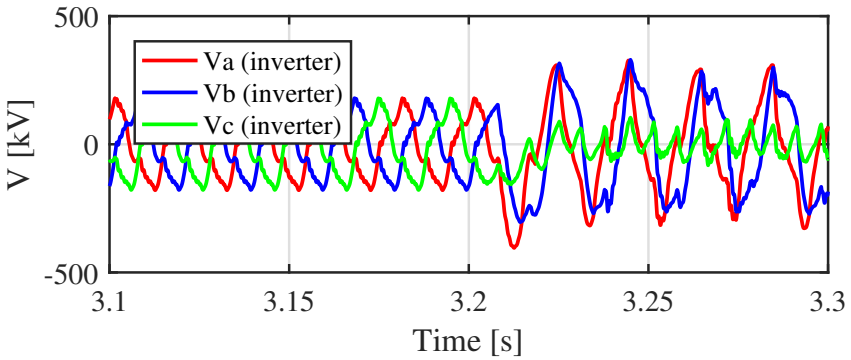

Figure 6.40: Voltage waveforms at the inverter AC terminals

Figures 6.42 and 6.43 show the effect of the commutation failure on the DC side of the inverter. Note that the commutation failure causes the DC inverter voltage to collpase, which implies

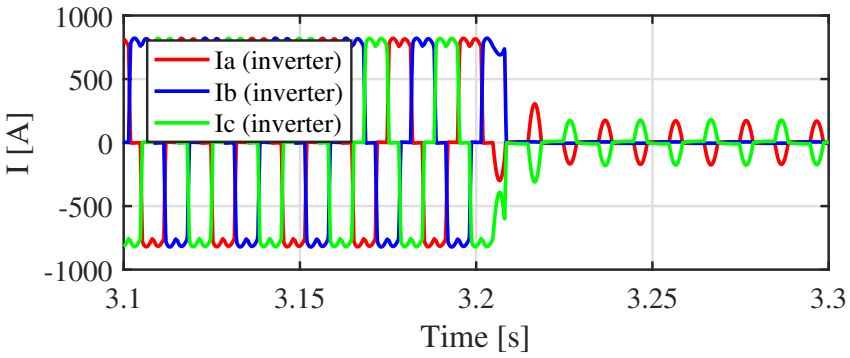

Figure 6.41: Current waveforms at the inverter AC terminals

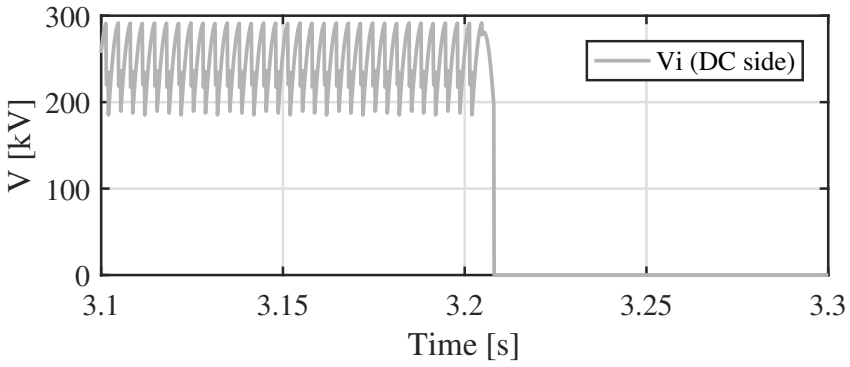

Figure 6.42: Voltage waveform at the inverter DC terminals

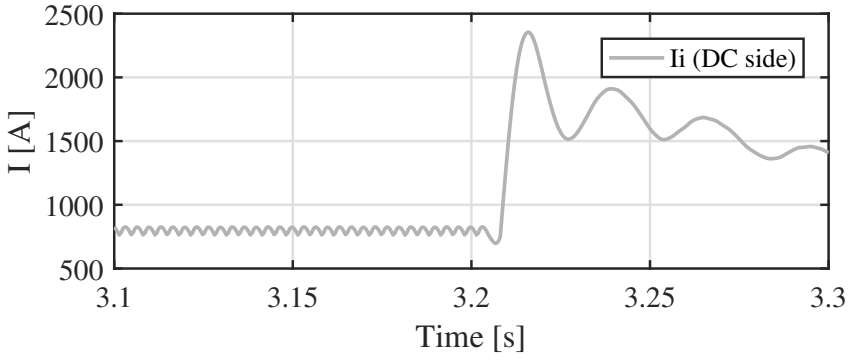

Figure 6.43: Current waveform at the inverter DC terminals

that the current through the DC link rises to high values (at the voltage diference between both poles suddenly increases), that could be hazardous to the system.

It is interesting to see the rectifier response through this contingency on the inverter side. Of course, the voltage collapse at the inverter terminal implies the termination of the power flow at the inverter terminals. However, as it can be seen in fig. 6.44, the rectifier control system tries to maintain the current at 800 A, maintaining a certain power flow. However, as the inverter votlage has collapsed, the power flowing through rectifier terminals will only feed the DC resistances of the cable, with potentially undesired consequences.

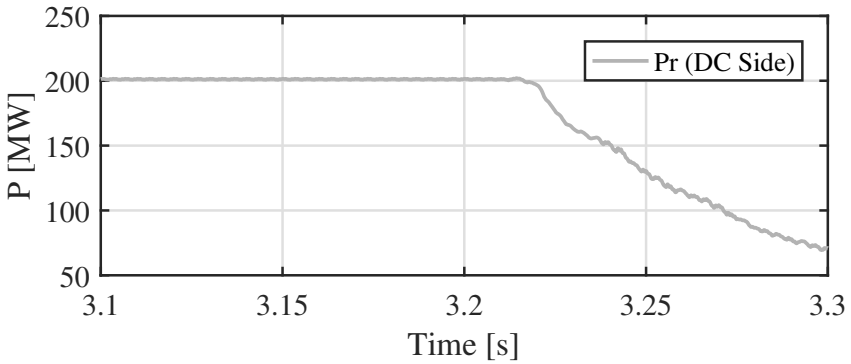

Figure 6.44: Active power measured at the DC rectifier terminals

In summary, it has been shown how a contingency on the AC inverter side of the system can trigger a low SCR condition, low enough to provoke a commutation failure by increasing the commutation time (i.e., increasing the commutation angle μ). This has caused a voltage collapse on the inverter DC side, which interrupts the power flow at the inverter side but not the power flow at the rectifier side, thereby transferring power uniquely to the resistances of the transmission system.

6.6 Case study conclusions

It has been proven that the linearised system reproduces the behaviour of the non-linear model. Hence, the proposed small-signal model is considered to be a valid step in reproducing the behaviour of the LCC transmission system. Furthermore, it has been shown how the mathematical analysis of the space-state representation of the model may contribute to deepen the understanding of stability issues in LCC transmission systems. Moreover, the time-domain simulation with a low SCR condition contributes to showing how contingencies on the AC side of one converter may affect the whole transmission system in a weak grid situation.

Conclusions

This thesis has exposed the theoretical background (commutation process, static curves and system operation) needed to understand and build a valid model of an LCC-HVDC transmission system. On the other hand, the goals set at the beginning of the thesis can be considered to be accomplished:

- The working principles of LCC-HVDC have been properly understood. Moreover, the static curves have been deeply analysed, and the construction of the small-signal model in conjunction with the non-linear model has been determinant in understanding the dynamic behaviour.
- The small-signal model has been tested in various situations. First of all, its results are concordant with the results yielded by the non-linear model. Moreover, it displays the expected behaviour for low SCRs, confirming the validity of this model.
- Potentially hazardous dynamic modes have been identified for particular cases.

As future work, the model could be expanded with phase-locked loop dynamics, which account for the variations between the measured apparent frequency and the real grid frequency. This should lower the stability range of the system.

Furthermore, the small-signal model will serve in future stability studies when linked with other similar models displaying power system, thereby studying the small-signal stability of a determinate system on a larger scale.

Acknowledgements

In the first place, I would like to thank Eduardo Prieto and Oriol Gomis for their dedication, help and support to the realisation of this thesis. Furthermore, I would like to thank Enric, Ricard and Marc for all the questions that they have solved and their support throughout the thesis.

Thanks to my family for their support, and especially to Sofia, as you have dealt with myself when building this work. Your support and love is beyond what I could ask for.

Appendix A

Environmental Impact

This section examines the environmental impact issued from the major applications of LCC and HVDC transmission in general; which correspond to offshore wind and power transmission. Despite not being directly related to this project, offshore wind is one of the main applications of HVDC, and serves to illustrate the indirect environmental impact of HVDC.

A.1 Environmental impact of HVDC transmission

A.1.1 Cable laying process

During the installation of HVDC sub-sea transmission, to prevent possible landslides on the seabed, as necessary to carry out excavations to install the cables. The ground excavation can cause a significant impact on the marine ecosystem.
The damage is particularly sensitive in cases where the excavation area contains endangered species, such as coral colonies. In this case, the excavation will not be realized, and should find an alternative route.
The boats used to carry out the installation of cables consume a significant amount of fuel and emissions of these boats damage the environment. It is to be noted that at sea, restrictions on emissions are more permissive in general than in land, and therefore emissions can have a greater relative impact.

A.1.2 Power efficiency

Regarding power efficiency, HVDC has a positive environmental impact. Compared to an equivalent AC link, HVDC transmission has generally lower losses, up to a half of the AC losses [14]. For instance, for a 200MW HVDC transmission system, assuming a CO2 equivalent coefficient of 0.5 KgCO2/kWh, aroud 6500 tons of carbon dioxide are saved up yearly, compared to an alternative HVAC transmission.

A.2 Environmental impact of offshore wind farms

A.2.1 Construction phase

First, in the construction phase, the seabed is disturbed by the foundations that have been built to withstand the wind turbines, which can modify the living ecosystem around the area, decisively affecting its development. Apart from that, the construction of wind turbines involve the use of heavy machinery, producing emissions that such machines entails: CO2 favors the greenhouse effect and toxic gases such as carbon monoxide or various sulfides. This machinery emits large amounts of noise that can affect the area.

A.2.2 Operational phase

When choosing the installation site of the wind farm, routes of marine life in the area and migratory routes of birds should also be considered, to minimize the impact on the ecosystem and in particular the possible collisions of birds with wind turbine blades.
Due to possible interactions with aircrafts or maritime routes, some safety measures have to be considered: visual flashy signs to prevent collisions with wind turbines.
In the operation phase generators emit no pollutants nor CO2. The issuance of such substances should only be counted in the phases of installation and dismantling.
As for the impact on the Earth's population, this may prove to be very small to null because of the great distances that generally separate offshore wind farms from the shore.

A.2.3 Dismantling phase

This phase begins when the turbine stops working properly and must be dismantled. This phase, although not overly difficult, requires the use of specialized machinery and as in the installation phase, machinery entails issuing certain amounts of CO2. The seabed can also be affected. This stage is accomplished minimizing the environmental impact on the ecosystem, identifying materials that could be reused to introduce them in the recycling chain.

Appendix B

Budget

The budget of this thesis accounts for research and development of this present work, as well as involved office equipment and software.

B.1 Labour costs

Labour costs are divided respectively in research hours, development hours and writing hours, assuming the salary of a junior researcher at 40e/h.

Concept	**Hourly rate[€/h]**	**Units** (h)	**Cost**(€)
Research	40	200	8000
Simulation and development	40	150	6000
Writing	40	200	8000
Subtotal		550	22000
VAT(21%)			4620
Total			26620

Table B.1: Labour costs

B.2 Developement tools and office material

This cost item includes the necessary tools to develop this project. The cost of IEEE articles or other literature material is not included, as the university provides free access to those contents.

B.3 Total cost

Considering the previous items, total cost can be seen in table B.3.

Concept	**Unit cost[€/ut]**	**Units**	**Cost(€)**
Personal computer	800	1	800
Matlab®2015 (Academic use)	500	1	500
Subtotal			1300
VAT(21%)			273
Total			1573

Table B.2: Development costs

Item	**Cost[€]**
Labour	26620
Development	1573
Total (VAT included)	**28173**

Table B.3: Total cost

Data: Twentieth of June, 2017 .
Signature: Joaquín Rebled Lluch.

Appendix C

Park Transformation

Time-dependency of electrical magnitudes expressed in their sinusoidal nature may hinder the capacity to control them. For this reason, it us usual to express *abc* magnitudes in the sinchronous $qd0$ reference frame, yielding constant magnitudes which allow for easier control design and signal observation. The mathematical transoformation from the *abc* frame to the $qd0$ frame is Park transformation.

The transformation is given by the following equations:

$$[x_{qd0}] = T(\theta)\,[x_{abc}] \tag{C.1}$$

where $T(\theta)$ corresponds to:

$$T(\theta) = \frac{2}{3}\begin{bmatrix} \cos(\theta) & \cos(\theta - \frac{2\pi}{3}) & \cos(\theta + \frac{2\pi}{3}) \\ \sin(\theta) & \sin(\theta - \frac{2\pi}{3}) & \sin(\theta + \frac{2\pi}{3}) \\ \frac{1}{2} & \frac{1}{2} & \frac{1}{2} \end{bmatrix} \tag{C.2}$$

Being $T(\theta)$ an invertible matrix, it is possible to perform the anti-transformation from the $dq0$ reference frame to the *abc* reference frame:

$$[x_{abc}] = T(\theta)^{-1}\,[x_{dq0}] \tag{C.3}$$

Where $T(\theta)^{-1}$ corresponds to:

$$T(\theta)^{-1} = \begin{bmatrix} \cos(\theta) & \sin(\theta) & 1 \\ \cos(\theta - \frac{2\pi}{3}) & \sin(\theta - \frac{2\pi}{3}) & 1 \\ \cos(\theta + \frac{2\pi}{3}) & \cos(\theta + \frac{2\pi}{3}) & 1 \end{bmatrix} \tag{C.4}$$

Appendix D

Details of the simulated systems within MATLAB® environment

The following figures show screenshots of the models employed in the case study, with the simulations performed in MATLAB®-Simulink.

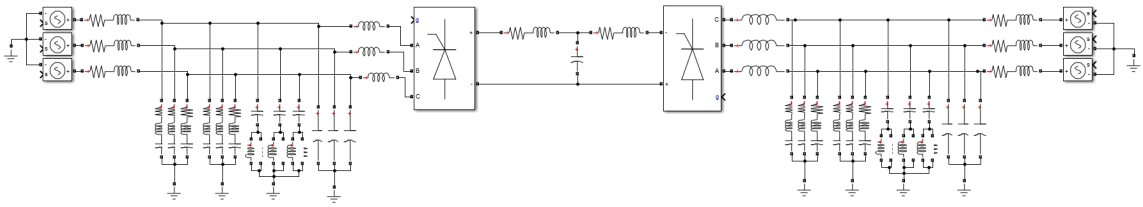

Figure D.1: Screenshot of the non-linear model

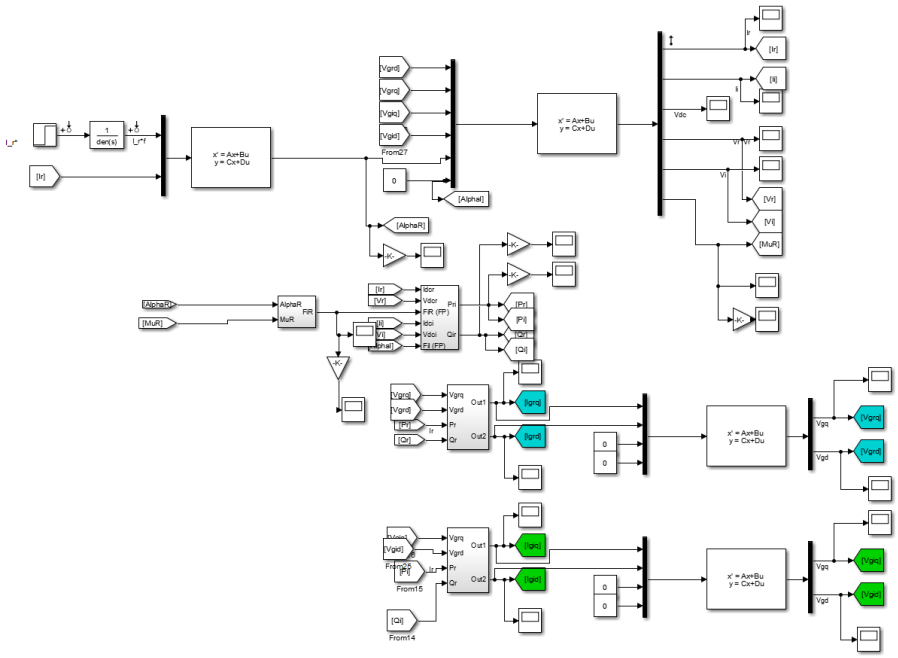

Figure D.2: Screenshot of the small-signal model

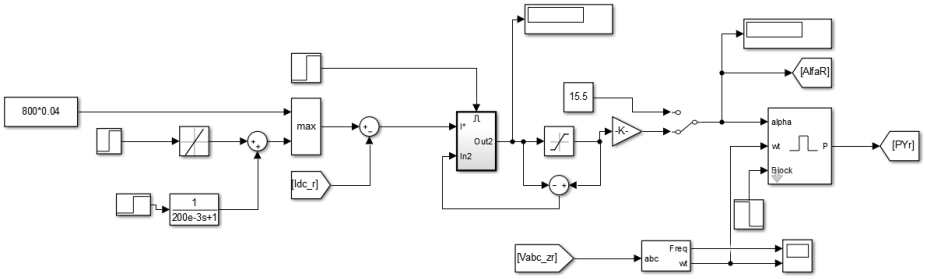

Figure D.3: Screenshot of the control system for the rectifier current control mode, in the non-linear model

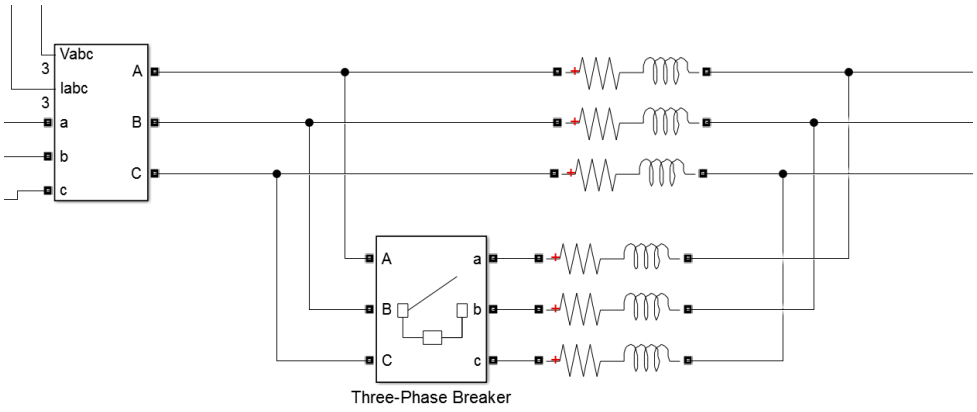

Figure D.4: Screenshot of the system used to trigger a low SCR condition, in the non-linear model

Bibliography

[1] ALSTOM (Firm). *HVDC: Connecting to the Future*. Alstom Grid, 2010. 15, 20, 24, 26, 27, 29

[2] W. Long and S. Nilsson. Hvdc transmission: yesterday and today. *IEEE Power and Energy Magazine*, 5(2):22–31, March 2007. 15, 16

[3] Rodrigo Teixeira Pinto. *Multi-Terminal DC Networks System Integration, Dynamics and Control*. PhD thesis, Delft University of Technology, 2014. 16

[4] Oluwafemi Oni, Kamati Mbangula, and Innocent Davidson. A review of lcc-hvdc and vsc-hvdc technologies and applications. *Transactions on Environment and Electrical Engineering*, 1(3):68–76, 2016. 16, 17

[5] D. Jovcic and K. Ahmed. *High Voltage Direct Current Transmission: Converters, Systems and DC Grids*. Wiley, 2015. 16, 20, 22, 23, 45

[6] S. Norrga. Hvdc - past , present and future. In *4th European Conference on Power Electronics and Applications*, 2011. 16

[7] J. Napoles, J. I. Leon, R. Portillo, L. G. Franquelo, and M. A. Aguirre. Selective harmonic mitigation technique for high-power converters. *IEEE Transactions on Industrial Electronics*, 57(7):2315–2323, July 2010. 16

[8] Eduardo Prieto Araujo. Power converter control for offshore wind energy generation and transmission. 2016. 17

[9] D. Van Hertem, O. Gomis-Bellmunt, and J. Liang. *HVDC Grids: For Offshore and Supergrid of the Future*. IEEE Press Series on Power Engineering. Wiley, 2016. 17

[10] UK Jones Alstom Grid, Stafford and C.C Davidson. Calculation of power losses for mmc-based vsc hvdc stations. In *15th European conference on Power Electronics and Applications*, 2013. 17

[11] P Venkatesh and MN Dinesh. Harmonic analysis of 6-pulse and 12-pulse converter models. *International Journal of Modern Engineering Research (IJMER)*, 1(4):31–36, 2014. 24

[12] Akagi, H. [et al.]. Generalized theory of instantaneous reactive power and its application. *Electrical Engineering in Japan*, 103(4):58–66, July 1983. 44

[13] M. O. Faruque, Yuyan Zhang, and V. Dinavahi. Detailed modeling of cigre hvdc benchmark system using pscad/emtdc and psb/simulink. *IEEE Transactions on Power Delivery*, 21(1):378–387, Jan 2006. 51

[14] N Barberis Negra, Jovan Todorovic, and Thomas Ackermann. Loss evaluation of hvac and hvdc transmission solutions for large offshore wind farms. *Electric power systems research*, 76(11):916–927, 2006. 85

[15] Sanchez, E. Disseny i implementacio d'un emulador de xarxa electrica. *Universitat Politecnica de Catalunya*.

[16] Egea-Alvarez, A., Junyent-Ferre, A., and Gomis-Bellmunt, O. *Active and reactive power control of grid connected distributed generation systems*.

[17] Chung, S. A phase tracking system for three phase utility interface inverters. *IEEE Transactions on Power Electronics*, 15(3):431–438, May 2000.

[18] Kazmierkowski, M.P., Krishnan, R, and Blaabjerg, F. Control in Power Electronics | 978-0-12-402772-5 | Elsevier.

[19] R. H. Park. Two-reaction theory of synchronous machines generalized method of analysis-part I. *Transactions of the American Institute of Electrical Engineers*, 48(3):716–727, July 1929.

[20] Verband der Elektrotechnik, Elektronik und Informationstechnik. VDE-AR-N 4105, 2011.

[21] A. Muthusamy and Chalmers tekniska högskola. Institutionen för energi och miljö. *Selection of Dynamic Performance Control Parameters for Classic HVDC in PSS/E: Optimization of CCA and VDCOL Parameters*. Chalmers University of Technology, 2010.

[22] C. Guo, Y. Zhang, A. M. Gole, and C. Zhao. Analysis of dual-infeed hvdc with lcc 2013;hvdc and vsc 2013;hvdc. *IEEE Transactions on Power Delivery*, 27(3):1529–1537, July 2012.

[23] H. Saad, S. Dennetiere, and B. Clerc. Interactions investigations between power electronics devices embedded in hvac network. In *13th IET International Conference on AC and DC Power Transmission (ACDC 2017)*, pages 1–7, Feb 2017.

[24] *Power System Stability And Control*. EPRI power system engineering series. McGraw-Hill Education (India) Pvt Limited, 1994.

[25] J. Machowski, S. Robak, P. Kacejko, P. Miller, and M. Wancerz. Short-circuit power as important reliability factor for power system planning. In *2014 Power Systems Computation Conference*, pages 1–8, Aug 2014.

[26] Y. Zhang. *Investigation of Reactive Power Control and Compensation for HVDC Systems*. University of Manitoba, 2011.